PERGAMON

Journal of Structural Geology 23 (2001) 693–713

JOURNAL OF STRUCTURAL GEOLOGY

www.elsevier.nl/locate/jstrugeo

Evidence of Early Cretaceous collisional-style orogenesis in northern Fiordland, New Zealand and its effects on the evolution of the lower crust

Nathan R. Daczko*, Keith A. Klepeis, Geoffrey L. Clarke

School of Geosciences, Division of Geology and Geophysics, Building F05, University of Sydney, Sydney, NSW 2006, Australia

Received 6 August 1999; revised 15 July 2000; accepted 26 July 2000

Abstract

Structural, metamorphic, and kinematic data from a well-exposed section of lower crustal rocks in northern Fiordland, New Zealand, reveal a history of intense contractional deformation and high-*P* metamorphism at the roots of a convergent orogen. High-*P* (>14 kbars) granulite facies garnet–clinopyroxene-bearing reaction zones occur adjacent to anorthositic veins within gabbroic and dioritic gneiss. These veins and reaction zones were variably deformed by two phases of high-*P* granulite facies deformation. Quantitative kinematic analyses, conducted using systems of rotated veins and reaction zones, indicate that the first phase produced steeply dipping shear zones within a sinistral pure-shear-dominated flow regime ($W_k = 0.69$). This deformation occurred at conditions of $P = 14.0 \pm 1.3$ kbars and $T = 676 \pm 34$°C and resulted in subhorizontal, arc-parallel (NE–SW) stretching and up to 60% subhorizontal shortening in high strain zones of the lower crust at depths >45 km. The second phase of deformation occurred at $P = 14.1 \pm 1.2$ kbars and $T = 674 \pm 36$°C and produced vertically stacked, gently dipping ductile thrust faults that accommodated arc-normal (NW-directed) displacement. These features reflect major tectonic thickening of the crust, oblique convergence, and high-*P* metamorphism during the collision of the roots of a convergent orogen, represented by plutons of the Median Tectonic Zone in eastern Fiordland, with the paleo–Pacific margin of Gondwana, represented by western Fiordland. Distinctive kinematic styles suggest that this collision resulted in a partitioning of the arc-parallel (NE–SW) and arc-normal (NW–SE) components of oblique convergence onto sinistral strike-slip and ductile thrust faults, respectively, at lower crustal levels.

1. Introduction

Interpreting the origin and evolution of penetratively deformed, high-pressure (>12 kbars) metamorphic belts is important for determining the response of the lower crust to plate convergence, collisional orogenesis, arc-related plutonism and many other types of tectonic activity. However, in many regions, especially in ancient metamorphic terranes where plate tectonic settings are ill-defined, interpretations of the tectonic significance of polyphase metamorphic and deformation events can be equivocal (e.g., see discussions by Wallis, 1995; Tikoff and Saint Blanquat, 1997; Klepeis and Crawford, 1999). In addition, studies of deformation processes in the lower crust are hindered by problems such as the uncertain effects of changing pressure, temperature, mineralogy, grain size, and rheology on the evolution of shear zone systems with increasing depth (e.g., Simpson and De Paor, 1993; Passchier and Trouw, 1995). In this paper, we present new structural, finite strain, kinematic and metamorphic data from lower crustal exposures in Fiordland, New Zealand (F, Fig. 1a), that help constrain the tectonic setting and effects of polyphase metamorphism and deformation on the evolution of a young, Cretaceous granulite facies belt whose development has been the subject of debate.

The northern and central parts of Fiordland in southwest New Zealand (Fig. 1) are comprised of over 10,000 km^2 of variably deformed, Paleozoic to Early Cretaceous, basic to intermediate orthogneisses that contain garnet–pyroxene–plagioclase mineral assemblages indicative of high pressure (>12 kbars) granulite facies metamorphism (Blattner, 1976; Oliver, 1977; Oliver and Coggon, 1979; Gibson et al., 1988; Bradshaw, 1989a). Previous studies of the granulites and other Fiordland rocks collectively point to several uncertainties surrounding the relative roles of tectonic and magmatic processes in the evolution of this high-grade metamorphic belt. Using conventional U–Pb zircon dating (Mattinson et al., 1986; McCulloch et al., 1987), and estimates of pressure–temperature (*P–T*) paths, Bradshaw (1989a, 1990) and Bradshaw and Kimbrough (1989) inferred a metamorphic history that was related to the

* Corresponding author.
E-mail address: ndaczko@mail.usyd.edu.au (N.R. Daczko).

0191-8141/01/$ - see front matter
PII: S0191-8141(00)00130-9

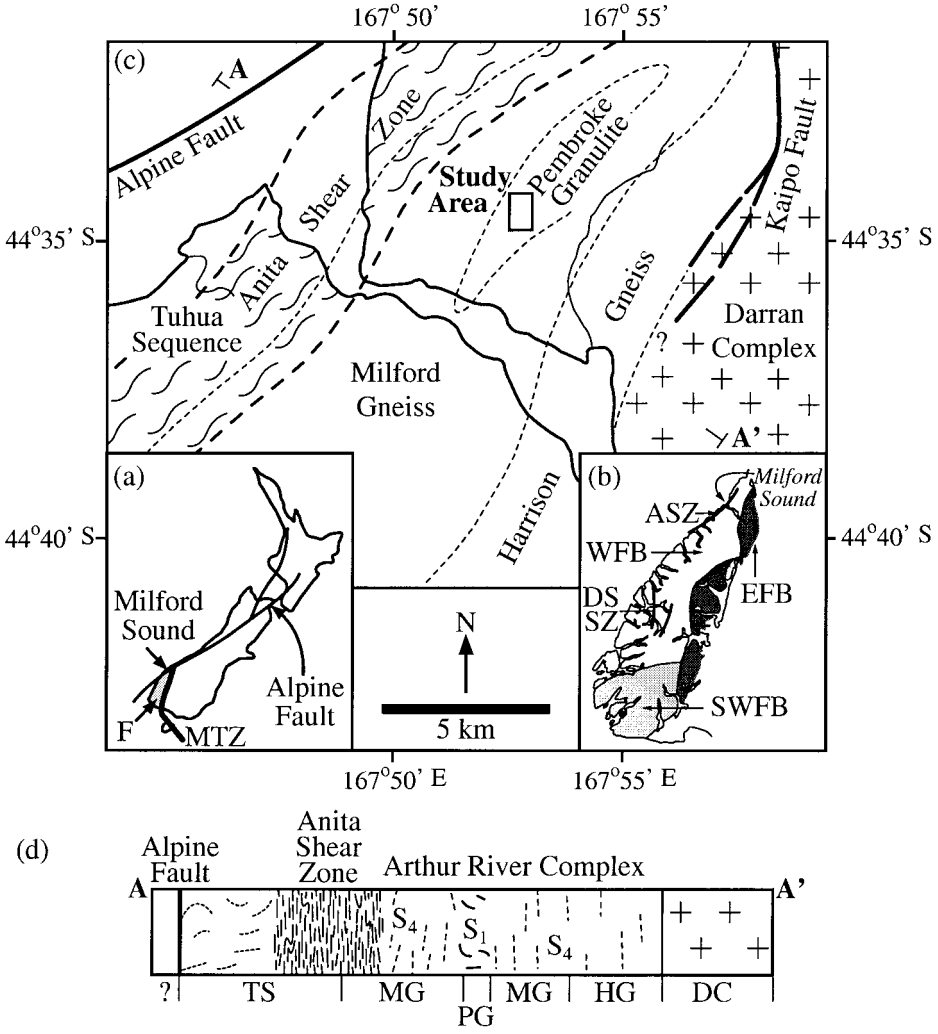

Fig. 1. (a) Map of New Zealand showing location of Alpine Fault, Fiordland (F, shaded region), and Median Tectonic Zone (MTZ, thick black line). (b) Map of Fiordland showing tectonic subdvisions: WFB–western Fiordland belt; EFB–eastern Fiordland belt; SWFB–southwest Fiordland block (after Bradshaw, 1990); ASZ–Anita Shear Zone; DSSZ–Doubtful Sound shear zone. (c) Geological map of Milford Sound area in northern Fiordland showing major lithologic divisions (after Blattner, 1991). (d) Cross-section (A–A′, in (c)) constructed for northern shore of Milford Sound. TS–possible Paleozoic Tuhua Sequence; MG–Milford Gneiss; PG–Pembroke Granulites; HG–Harrison Gneiss; DC–Darran Complex.

Cretaceous emplacement of a major calc–alkaline batholith within an arc–continent collisional setting. An increase in pressure with time also suggested to these investigators that low- to medium-*P* granulite facies metamorphism occurred prior to Early Cretaceous collisional orogenesis and loading (see also Bradshaw, 1989). Oliver (1990) and Brown (1996), however, both inferred that these high-grade metamorphic conditions and the increase in pressure during metamorphism in Fiordland were produced by magma loading following the mid-crustal emplacement of Cretaceous dioritic and gabbroic plutons of the Western Fiordland Orthogneiss. Muir et al. (1995, 1998) used geochemical and geochronologic data to argue that an Early Cretaceous magmatic arc, chemically equivalent to the Darran Complex in eastern Fiordland (Fig. 1c), was thrust beneath western Fiordland to depths >40 kms and melted to produce the Western Fiordland Orthogneiss. This latter interpretation implies that Fiordland experienced arc–continent collision and large-scale tectonic thickening of the middle and lower crust prior to at least some granulite facies metamorphism. Finally, Gibson and Ireland (1995) and Ireland and Gibson (1998) suggested that some granulite facies metamorphism in Fiordland occurred during regional continental extension at ~107 Ma. This interpretation implies that granulite facies metamorphism outlasted subduction- and collision-related pluton emplacement at lower crustal levels and continued within a mid-Cretaceous extensional regime that led to the rifting of New Zealand from Gondwana.

In this paper, we present the first direct structural and kinematic evidence of major tectonic thickening, lower crustal thrust faulting, and sinistral pure-shear-dominated flow following Early Cretaceous pluton emplacement within the northern part of the western Fiordland belt (WFB, Fig. 1b). Our analyses allowed us to test previously

proposed hypotheses of the roles and effects of tectonic processes on the evolution of high-*P* granulites and plutons in western Fiordland. We determined the type, amount, and kinematics of lower crustal deformation by using outcrop-scale variations in strain intensity and changes in the rotation history of three sets of anorthositic veins and granulite facies reaction zones. The reaction zones form excellent passive strain markers that indicate the granulites were affected by sinistral pure-shear-dominated flow that caused up to 60% subhorizontal shortening of the lower crust in high strain zones, major ductile thrust faulting, and tectonic thickening at lower crustal levels. These results suggest that the high-*P* metamorphism and deformation in northern Fiordland occurred within a setting characterized by oblique sinistral convergence and arc–continent collision. Collision occurred between the eastern and western provinces of Fiordland prior to the onset of regional extension and ductile normal faulting at ~108 Ma (age of extension from Tulloch and Kimbrough, 1989). Finally, we show that structures formed during granulite facies metamorphism subsequently exerted a strong degree of control on ductile flow and the partitioning of deformation within the lower crust.

2. Regional geologic history

The western belt of Fiordland (WFB, Fig. 1b) preserves a history of mid-Paleozoic convergent margin deformation, polyphase metamorphism, and plutonism that occurred when ancestral New Zealand lay within or outboard of the paleo–Pacific margin of Gondwana (Wood, 1972; Carter et al., 1974; Oliver, 1990; Gibson and Ireland, 1996; Mortimer et al., 1999). U–Pb SHRIMP microprobe dates (Ireland and Gibson, 1998), Rb–Sr isochron ages (Oliver, 1980) and K–Ar cooling ages (Gibson et al., 1988) suggest that this tectonism lasted from ~481 Ma to ~334 Ma in western Fiordland (Gibson et al., 1988; Gibson and Ireland, 1996; Ireland and Gibson, 1998). At least two distinctive Paleozoic metasedimentary sequences occur in the western Fiordland belt. The first sequence may be equivalent to Early Paleozoic rocks of the Delamerian fold belt (Gibson and Ireland, 1996). The second sequence may represent part of the Tuhua Sequence (Fig. 1c) which includes rocks as old as Cambrian exposed in the northwest part of New Zealand's South Island (Wood, 1972; Bradshaw, 1990).

Following Paleozoic tectonism and prior to the initiation of an extensional regime in the mid-Cretaceous, western Fiordland experienced several additional phases of high-grade metamorphism, deformation and arc-related plutonism (Bradshaw, 1989; Bradshaw, 1989a; Tulloch and Kimbrough, 1989; Oliver, 1990; Mortimer, 1993; Brown, 1996). These phases overlapped in time with the Triassic to Early Cretaceous accretion of outboard terranes onto the Pacific margin of Gondwana and with the emplacement of a regionally extensive calc–alkaline batholith (Mattinson et al., 1986; McCulloch et al., 1987; Tulloch and Kimbrough, 1989; Oliver, 1990; Mortimer et al., 1999). In Fiordland, this batholith includes a suite of variably deformed and metamorphosed 126–119 Ma metadiorites and metagabbros called the Western Fiordland Orthogneiss. Following their emplacement, rocks of the Western Fiordland Orthogneiss were affected by high-*P* granulite facies metamorphism peaking at temperatures of 650–700°C and pressures of 12–13 kbars (Bradshaw, 1989a; Brown, 1996; Gibson et al., 1988; Gibson and Ireland, 1995).

During the Early Cretaceous, the Western Fiordland Orthogneiss intruded the Arthur River Complex in northernmost Fiordland (Bradshaw, 1990). The Arthur River Complex is a heterogeneous assemblage of orthogneisses and dikes of Early Mesozoic and possibly also Paleozoic protolith age (Mattinson et al., 1986; Bradshaw, 1990) and is subdivided into the mafic Pembroke Granulites and Milford Gneiss and the dioritic Harrison Gneiss (Fig. 1c, d; Wood, 1972; Blattner, 1991). The Arthur River Complex also experienced high-*P* (>14 kbars) granulite facies metamorphism similar to the Western Fiordland Orthogneiss (Blattner, 1976; Oliver, 1977; Bradshaw, 1990; Turner, 1998; Clarke et al., 2000). The western boundary of the Arthur River Complex comprises the Anita Shear Zone (Hill, 1995a,b). This shear zone is a 4 km-wide, long-lived Cretaceous to Early Tertiary structure that preserves a polyphase history of deformation and metamorphism. High-grade, mylonitic fabrics were produced by mid-Cretaceous or younger ductile normal faulting (Klepeis et al., 1999). These fabrics are overprinted by pure-shear-dominated dextral fabrics of uncertain, but probable latest Cretaceous to Early Tertiary age (Klepeis et al., 1999). Both of these fabrics in the Anita Shear Zone cut all foliations preserved in the Milford Gneiss to the east.

East of the Anita Shear Zone, the dominant structure in the Milford and Harrison gneisses is a steeply east- to northwest-dipping foliation (Fig. 1d). This foliation is defined by flattened clusters of coarse amphibole and plagioclase grains with or without garnet, clinopyroxene, biotite and phengite. A weakly to strongly developed, steeply plunging mineral lineation defined mainly by the alignment of amphibole and plagioclase aggregates occurs on foliation planes. Near the contact between the Milford and Harrison gneisses, two-pyroxene, hornblende-bearing metagabbroic rocks preserve evidence of granulite facies metamorphism. These granulites are enveloped by the dominant *L–S* fabric of the Arthur River Complex (see also Blattner, 1991). The best exposures of these granulite facies orthogneisses occur in the Pembroke Valley located north of Milford Sound (Fig. 1c). We use these exposures to examine the earliest history of deformation and high-pressure metamorphism within the Arthur River Complex.

The Arthur River Complex has a gradational or faulted eastern contact with leucogabbros and diorites of the 141–137 Ma Darran Complex (Fig. 1c; Blattner, 1978, 1991). The Darran Complex forms part of the Median Tectonic Zone (MTZ; Table 1), a 10–35 km wide, NNE-trending

Table 1
Summary of abbreviations used in text

Abbreviation	Use
MTZ	Median Tectonic Zone
GRZ	Garnet Reaction Zone (refers to alteration zone)
GRZ_1	The east-striking set of Garnet Reaction Zones
GRZ_2	The north-striking set of Garnet Reaction Zones
GRZ_3	The northeast-striking set of Garnet Reaction Zones
D_1	Pervasive S_1–L_1 two-pyroxene-amphibole fabric
D_2	Fracturing and anorthositic veining event
D_3	Pervasive S_3–L_3 fabric in steeply dipping mylonites
D_4	Pervasive S_4–L_4 fabric in shallowly dipping mylonites (thrusts)

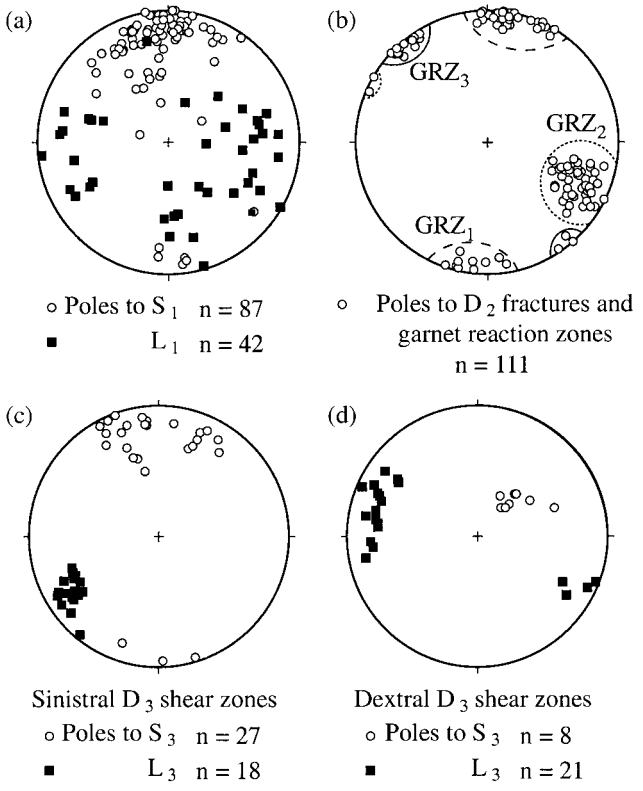

Fig. 2. Lower hemisphere equal area plots of structural data from the Pembroke Granulites. (a) D_1 elements (L_1 and poles to S_1). (b) Poles to three sets of subvertical fracture planes (D_2 elements) and associated planar GRZs (GRZ_1, GRZ_2, GRZ_3). (c) D_3 elements (L_3 and poles to S_3) from sinistral shear zones. (d) D_3 elements (L_3 and poles to S_3) from dextral shear zones.

belt of mid-Jurassic to Early Cretaceous plutons, minor metamorphosed volcanic rocks, and sedimentary units that were derived from a long-lived Mesozoic magmatic arc (Bradshaw, 1993; Kimbrough et al., 1994; Mortimer et al., 1999).

Following emplacement of the Darran Complex and the Western Fiordland Orthogneiss, widespread extension affected parts of western New Zealand by 108 Ma (Tulloch and Kimbrough, 1989) or 105 Ma (Bradshaw, 1989). This deformation has been interpreted to reflect the beginnings of the mid-Cretaceous breakup of Gondwana (Bradshaw, 1989; Tulloch and Kimbrough, 1989; Oliver, 1990). By late Tertiary time, changes in relative motions between the Pacific, Australian and Antarctic plates led to the development of the modern Australian–Pacific transform plate boundary (Sutherland, 1995; Lamarche et al., 1997). In southwestern New Zealand, this plate boundary is represented by the Alpine Fault (Norris et al., 1990).

3. Deformation and metamorphism in the Pembroke granulites

The oldest foliation (S_1) exposed in the Pembroke Valley occurs within heterogeneously deformed and metamorphosed gabbroic and dioritic plutons. S_1 commonly is defined by aligned, elongate mineral clusters cored by coarse orthopyroxene and clinopyroxene rimmed by amphibole and set in a coarse plagioclase matrix. In many places orthopyroxene and clinopyroxene grains are stable and exhibit magmatic textures defined by coarse, equant orthopyroxene aggregates with exsolution blebs of clinopyroxene and opaque phases. The orientation of S_1 is variable, but generally strikes east to east-northeast and displays steep to near-vertical dips to the south and SSE (Fig. 2a). A weakly developed, down-dip amphibole mineral lineation (L_1) plunges variably to the east and west on S_1 foliation planes (Fig. 2a).

3.1. Garnet reaction zones and anorthositic vein sets

The Pembroke Valley displays a network of vertical, planar fractures (D_2) that form a distinctive lattice pattern on horizontal surfaces (Fig. 3a). These fractures are commonly filled with anorthositic veins that everywhere cut the S_1 foliation (Fig. 3b). Adjacent to the veins, S_1 hornblende is statically pseudomorphed by finely intergrown garnet and clinopyroxene (bleached-looking areas in Fig. 3a, b). This replacement of the S_1 mineral assemblage by garnet and clinopyroxene produces a distinctive pink alteration band that we refer to here as a garnet reaction zone (GRZ; Table 1). These planar reaction zones were described in detail by Blattner (1976), Oliver (1977), and Bradshaw (1989b). Individual veins/reaction zones are typically

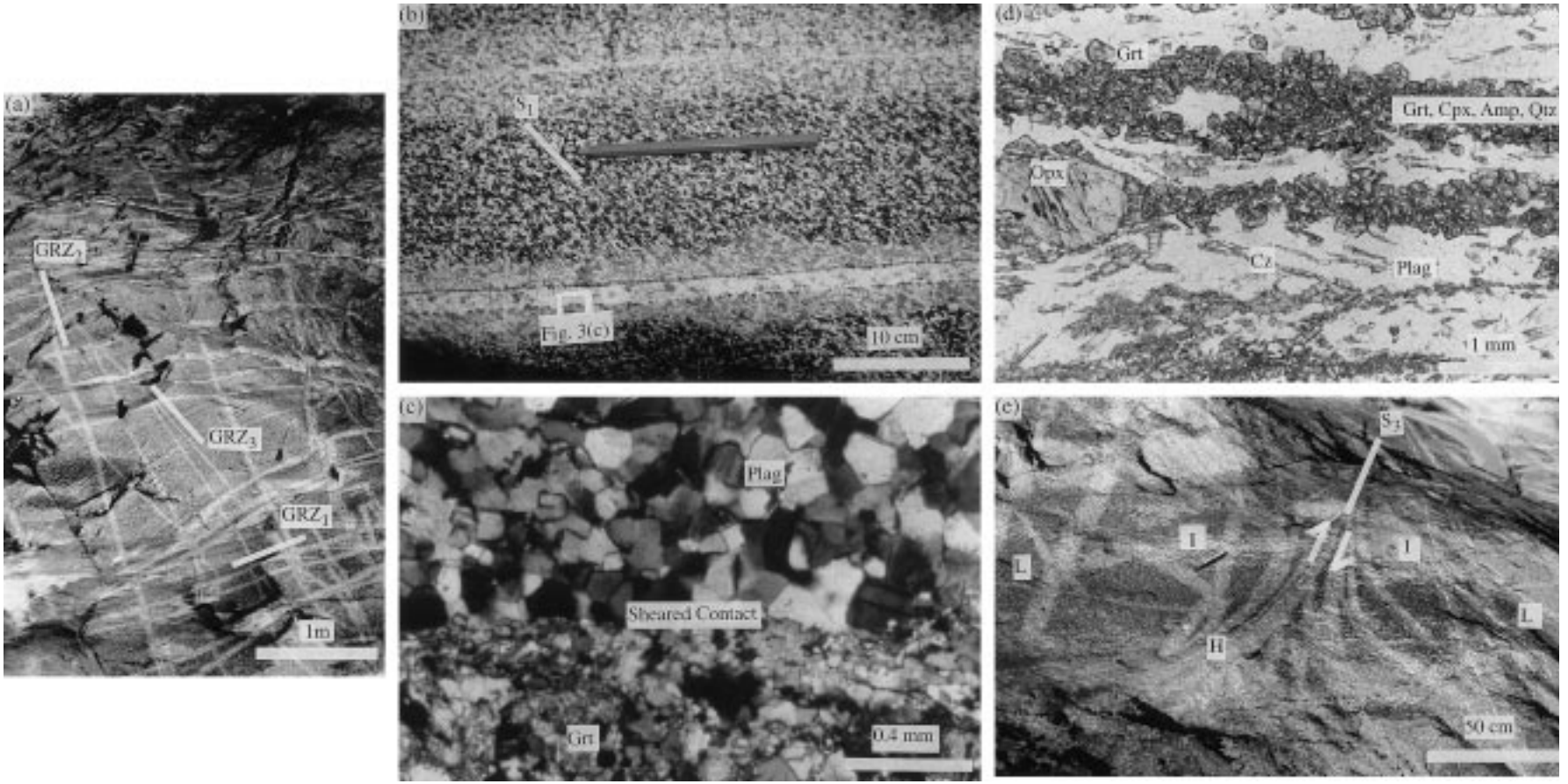

Fig. 3. (a) Outcrop photo of lattice pattern formed by three sets of D_2 fracture planes and surrounding GRZs (GRZ_1, GRZ_2, GRZ_3) on subhorizontal surface. (b) Photo showing S_1 foliation trending diagonally from top left to bottom right. Garnet and clinopyroxene statically pseudomorph S_1 forming a pink (shown white in photo) reaction zone that surrounds anorthositic veins. (c) Photomicrograph (crossed polarized light) showing texture of contact between an anorthositic vein (top) and an adjacent GRZ (bottom). See (b) for location. Note narrow zone of recrystallization and grain size reduction at the contact. (d) Photomicrograph (plain polarized light) showing attenuation of mafic clusters in a D_3 shear zone (surface oriented perpendicular to foliation and parallel to lineation). S_3 mineral assemblage is garnet (Grt), clinopyroxene (Cpx), amphibole (Amp), quartz (Qtz), clinozoisite (Cz), orthopyroxine (Opx) and plagioclase (Plag). (e) Outcrop photo showing northwest-striking dextral shear zone (D_3) and adjacent low (L), intermediate (I), and high (H) strain domains.

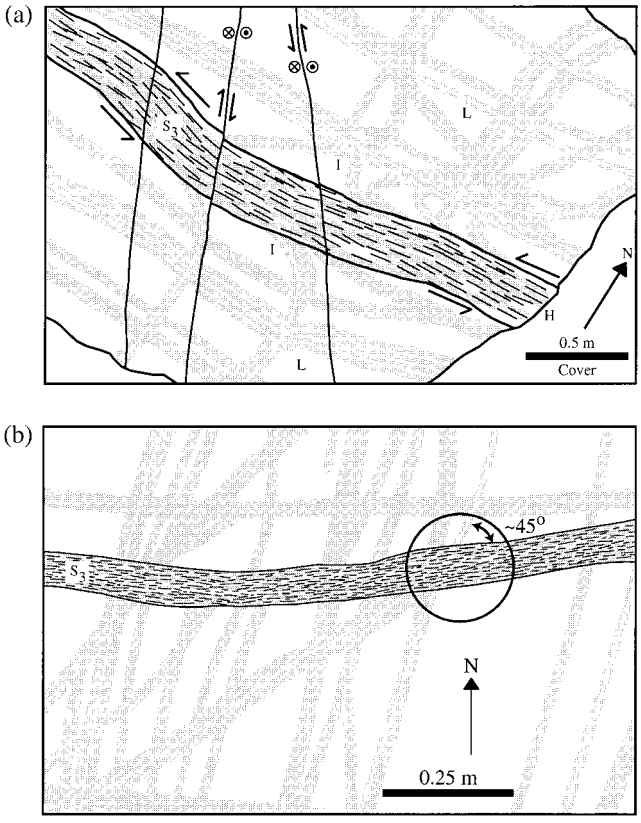

Fig. 4. (a) Sketch of a sinistral D_3 shear zone that deforms GRZs (shaded lines). Note well-defined shear zone boundaries. Reaction zones oriented at high angles to the boundaries are reoriented and transposed parallel to the shear zone in high strain domains (H). A lesser degree of reorientation occurs within intermediate strain domains (I). Little to no reorientation of reaction zones occurs within low strain domains (L). Note late semi-brittle faults that crosscut shear zones at a high angle. (b) Sketch of sinistral D_3 shear zone crosscutting GRZs. Circle highlights a GRZ_3 reaction zone that passes through the shear zone showing little to no rotation. Angle between reaction zone and shear zone boundaries is approximately 45°. See text for discussion of significance.

spaced less than 1 m apart and the reaction zones display widths of 1–5 cm although some zones are up to 10 cm wide. Individual reaction zones can be traced for distances of at least 50 m on subhorizontal surfaces. The most recent estimate of peak metamorphic conditions recorded by the pyroxene–garnet–plagioclase assemblages in the Pembroke Valley reaction zones is $P = 14–16$ kbar and $T = 750–850$°C (Turner, 1998; Clarke et al., 2000). A full description of the metamorphic evolution of the northern Fiordland granulites is presented in Clarke et al. (2000).

The lattice pattern formed by the GRZ reflects three subvertical sets of veins that are distinguishable only on the basis of their orientation. We use the acronym GRZ with a subscript 1, 2 or 3 to distinguish the three sets (Table 1). GRZ_1 are east-striking and display vertical to steep dips to the south (Figs. 2b, 3a). GRZ_2 intersect GRZ_1 at approximately 90° and strike to the north and NNE and dip very steeply to the west (Figs. 2b, 3a). GRZ_3 bisect the GRZ_1 and GRZ_2 sets at approximately 45°. GRZ_3 strike northeast and dip steeply to the southeast (Figs. 2b, 3a).

3.2. D_3 deformation and definition of strain domains

The GRZs in the Pembroke Valley are variably deformed by macroscopic garnet granulite facies shear zones that are commonly less than 1 m wide and have well-defined boundaries (Fig. 4). These shear zones (D_3) all contain a penetrative mylonitic foliation (S_3) defined by aligned and flattened amphibole, garnet and clinopyroxene aggregates within a plagioclase-rich matrix (Fig. 3d). In areas of the highest strain, S_3 everywhere parallels the boundaries of the shear zones. The GRZs and veins in these high strain domains were reoriented and transposed parallel to S_3 (Figs. 3e, 4). In low strain domains, GRZs and veins are completely unaffected by D_3 deformation. Domains of intermediate strain (20–40 cm wide) occur between low and high strain zones parallel to shear zone boundaries (Figs. 3e, 4a). Plagioclase in these domains displays evidence of incomplete dynamic recrystallization including sutured grain boundaries, strained crystal lattices, and minor to moderate dismemberment of mafic mineral clusters. GRZs in these intermediate strain domains have been weakly to moderately reoriented such that the acute angles between any two of the three orientations of reaction zones is significantly reduced compared to the angles displayed in low strain domains (Figs. 3e, 4a).

We divide the high strain domains of the D_3 shear zones into two sets on the basis of orientation, size, and abundance. The first and dominant set contains an east-striking, steeply south-dipping mylonitic foliation (S_3) that parallels GRZ_1 (compare Figs. 2b, c, 4a). A penetrative, gently southwest-plunging, mineral lineation (L_3), defined by attenuated clusters of amphibole and clinozoisite, occurs on S_3 foliation planes. Sense of shear indicators within this set (described below) are consistently sinistral. The second set is subordinate in size and abundance to the first group. S_3 within this second set is northwest-striking and displays shallow to moderate dips to the southwest (Fig. 2d). L_3 is a gently west and northwest-plunging amphibole and clinozoisite mineral lineation (L_3; Fig. 2d). Sense of shear indicators within the subordinate set are consistently dextral.

3.3. D_4 shear zones

Cutting all D_3 shear zones is a series of parallel, 1.5–4 m wide, gently southeast-dipping D_4 shear zones (Fig. 5). The latter have well-defined, narrow (~10 cm) boundaries and are spaced approximately 50–100 m apart in a vertical direction. Each contains an intensely developed, highly planar, gently southeast-dipping S_4 foliation defined by recrystallised and aligned amphibole, clinozoisite, garnet and biotite. Stretched aggregates of garnet and plagioclase and aligned amphibole grains define a penetrative down-dip, southeast-plunging mineral lineation (L_4) on S_4 foliation

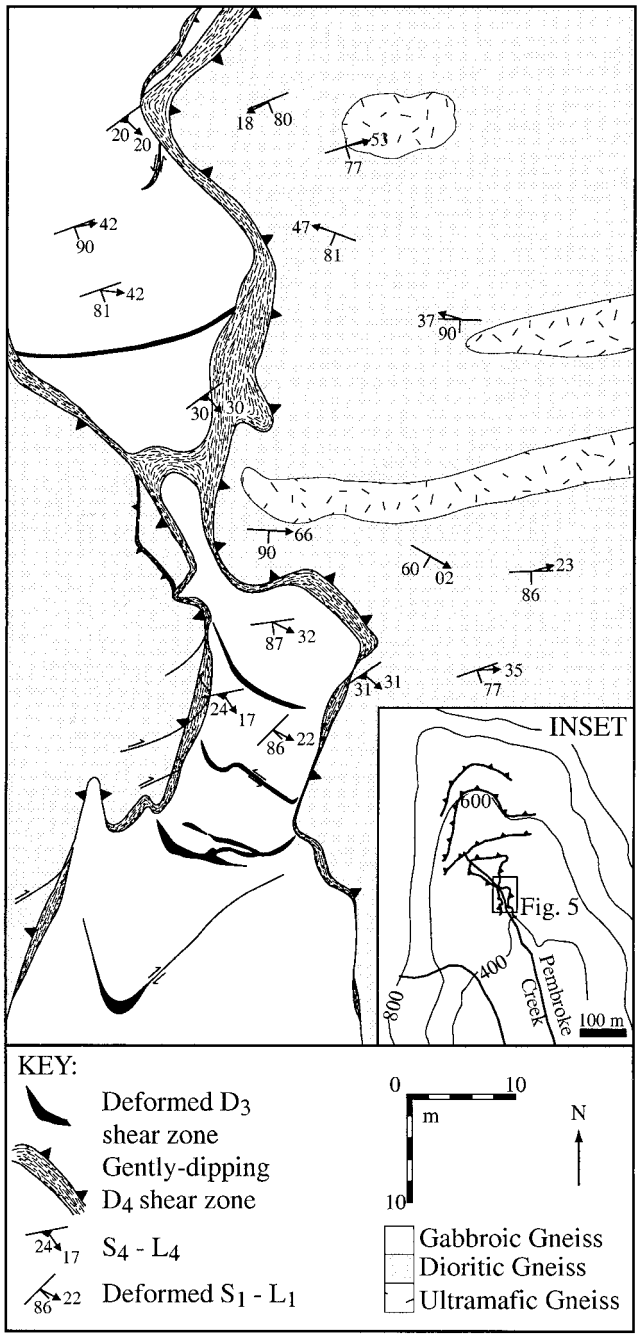

Fig. 5. Plan view sketch of D_4 ductile thrust fault and related structures. Inset shows pattern of vertically stacked, subhorizontal thrusts and their location within the Pembroke Valley. Numbers in inset refer to elevation (meters) above mean sea level.

planes. Within D_4 shear zones, all older fabrics are re-oriented and transposed into S_4. At the boundaries of these shear zones and also between a number of parallel shear zones, D_4 deformation produced steeply southeast- and northwest-dipping mylonitic shear bands that curve into and merge with the centers of the D_4 shear zones. Like the main shear zones, these shear bands crosscut all other structures, including the D_3 shear zones.

4. Kinematic and finite strain analysis of D_3

In this section we use spatial variations in the intensity of deformation that affected the GRZs to determine the kinematics of D_3 ductile flow. Our aims include the following: (1) to determine the bulk sense and directions of displacement associated with D_3 deformation; (2) to determine the type and kinematic vorticity of flow during D_3; (3) to estimate the amount of finite shortening of the lower crust associated with this deformation; and (4) to assess whether this deformation is consistent with tectonic models of transpression, transtension, contraction, and/or extension etc.

4.1. Description of deformation kinematics

A description of the kinematics of a deformation involves the determination of the following components: volume change, rotation, stretch and translation. The amount of translation is reference frame dependent. For constant volume deformation, we can describe the rate of rotation as the vorticity of flow. For general non-coaxial deformation, the relative contributions of the rotation rate and the stretching rate produce variable degrees of non-coaxiality. A useful means of describing the degree of non-coaxiality for a deformation is the kinematic vorticity number (W_k). For deformations involving plane strain, this quantity is a measure of the relative contributions of the simple shear and pure shear components such that $W_k = 0$ for wholly pure shear and $W_k = 1$ for wholly simple shear (Lister and Williams, 1983; Passchier, 1987; Passchier and Urai, 1988). Because pure shear deformation and simple shear deformation accumulate at different rates, W_k ranges from 0 to approximately 0.75 for pure shear-dominated deformation and from 0.75 to 1 for simple shear-dominated deformation (Tikoff and Fossen, 1995).

The GRZs exposed in northern Fiordland provide a means of estimating both the stretch component (R_f) and the kinematic vorticity number (W_k) of ductile flow for D_3 deformation. We discuss the possible effects of volume change later. We obtained estimates of these two parameters by measuring mesoscopic changes in the orientation, rotation direction, and magnitude of angular shear strain exhibited by the three sets of GRZs across low, intermediate and high D_3 strain domains. Evidence of both sinistral and dextral rotations in individual, dominantly sinistral shear zones indicated a significant deviation from simple shear.

For an accurate assessment of the strain and vorticity of flow, the GRZs must have behaved passively with their matrix. Close examination of the reaction zones in the Pembroke Valley indicated that these structures are virtually unaffected by buckle folds and boudinage despite evidence of large (>90°) rotations during D_3 deformation. This lack of visible buckle folds and boudinage appears be the result of a very low competency contrast between the reaction zones, veins and the surrounding matrix, indicating passive behavior. The low degree of competency contrast may

reflect the similar plagioclase-dominated compositions in both marker and matrix and/or the very high-grade conditions of deformation ($P = 14$ kbars, $T = 750$–850°C, discussed below). Previous studies (e.g., Ramsay and Huber, 1983; Passchier, 1990) have shown that low competency contrasts can allow strain markers to accommodate a significant amount of longitudinal shortening and extension without buckling or exhibiting boudinage. We observed that only in narrow (~5–8-cm-wide) zones near the boundaries between high and intermediate strain zones do the veins display evidence of pinch and swell. Even in high strain zones, however, these reaction zones do not display mesoscopically visible boudinage despite evidence of stretched and dismembered clusters of mafic minerals. The main effect of this stretching appears to be a thinning of individual reaction zones.

We use the array of different reaction zone orientations and variations in the sense and magnitude of the passive rotations they record with increasing degree of strain to estimate W_k. The basis of this analysis is that, within a general non-coaxial flow field undergoing plane strain, two flow apophyses exist that do not rotate with respect to the instantaneous stretching axes (e.g., Bobyarchick, 1986; Passchier, 1986; Wallis, 1992; Simpson and De Paor, 1993). For a thinning shear zone (i.e., sub-simple shear), one apophysis generally parallels the flow plane of the simple shear component of deformation or the shear zone boundaries (Simpson and De Paor, 1993). The other flow apophysis is inclined with respect to the shear zone boundaries. Material lines that lie on opposite sides of the inclined apophysis rotate in opposite directions. The acute angle (ν) between the two flow apophyses is dependent upon the amount of simple versus pure shear such that this angle is 90° for wholly pure shear and 0° for wholly simple shear. The angle ν is related to W_k as follows:

$$W_k = \cos(\nu) \quad (1)$$

(Bobyarchick, 1986; Passchier, 1986; Simpson and De Paor, 1993). Determination of the angle (ν) between the apophyses in a steady flow field thus allows determination of the kinematic vorticity of flow.

4.2. Estimate of a time-averaged W_k

We measured the orientation and rotation history of more than 250 GRZs over a 0.75 km^2 area, including 100 from low strain domains, 90 from intermediate strain domains and 60 from high strain domains. Many of these reaction zones were traced continuously from low strain domains into high strain domains. By tracing reaction zones across strain domain boundaries, we distinguished those that rotated sinistrally from those that rotated dextrally. Determination of the orientation of lines of no rotation yielded the orientations of the two flow apophyses. Measurement of the 250 reaction zones in three dimensions also indicated that all rotations within shear zones occurred within a plane oriented perpendicular to the three subvertical reaction zone sets. Rotation within a single plane, defined here as the flow plane, indicates that the deformation approximated plane strain conditions and justifies a two-dimensional analysis of kinematic vorticity. In accordance with this observation, no asymmetric microstructures such as recrystallized tails on porphyroclasts were observed in planes other than the flow plane.

We established the following trends: (1) Sinistral rotation during D_3 was dominant (Fig. 4a). This bulk sinistral shear sense was confirmed using microstructural evidence and asymmetric sense of shear indicators including C'-type shear bands (e.g., Passchier and Trouw, 1995), asymmetric recrystallized tails on feldspar porphyroclasts, fractured and microfaulted garnet grains, and oblique foliations (e.g. Fig. 8a). (2) In low strain domains, the angle between GRZ_1 and GRZ_2 is very close to 90° and the angle between GRZ_1 and GRZ_3 is approximately 45° (Figs. 2b, 3a, 4). (3) GRZ_1 reaction zones show little to no reorientation across strain domain boundaries (compare Fig. 6a, b, e); the other two sets rotated into approximate parallelism with GRZ_1 with increasing strain. These relationships indicate that the average orientation of GRZ_1 coincided with one of the flow apophyses for D_3 shear zones. This flow apophysis also parallels the boundaries of the dominant set of sinistral shear zones. Minor dextral shear zones (discussed below) also occur. (4) GRZ_2 displayed dominantly sinistral rotation with some minor dextral rotation (compare Fig. 6c, d, e). (5) GRZ_3 displayed approximately equal sinistral and dextral rotations (Fig. 6g). In addition, some GRZ_3 orientations did not rotate. These relationships indicate that the second flow apophysis coincided with the average orientation of GRZ_3 (Fig. 7). This second apophysis forms an angle of 43–47° with respect to the shear zone boundaries and the first apophysis (Fig. 7). On the basis of this angle, we obtained a kinematic vorticity number of $0.63 < W_k < 0.73$ (Eq. (1)) indicating a bulk sinistral pure-shear-dominated flow regime for D_3 deformation.

4.3. Test of vorticity results with site-specific measurements

Our estimate of W_k using the deformed reaction zones described above represents a result that is averaged over both the duration of D_3 deformation and over the 0.75 km^2 area of the Pembroke Valley. In this subsection, we describe an independent measure of W_k obtained for individual sinistral and dextral shear zones to test the assumption of steady state deformation and the validity of our time-averaged result.

Individual shear zones within the Pembroke Valley all contain abundant kinematic indicators. One of these indicators is a grain-shape foliation, defined by aligned amphibole and plagioclase aggregates, that lies oblique to both the shear zone boundaries and the main S_3 foliation (Fig. 8a). These oblique foliations commonly are preserved inside 10-cm-long, 5-cm-wide asymmetric pods that are enveloped

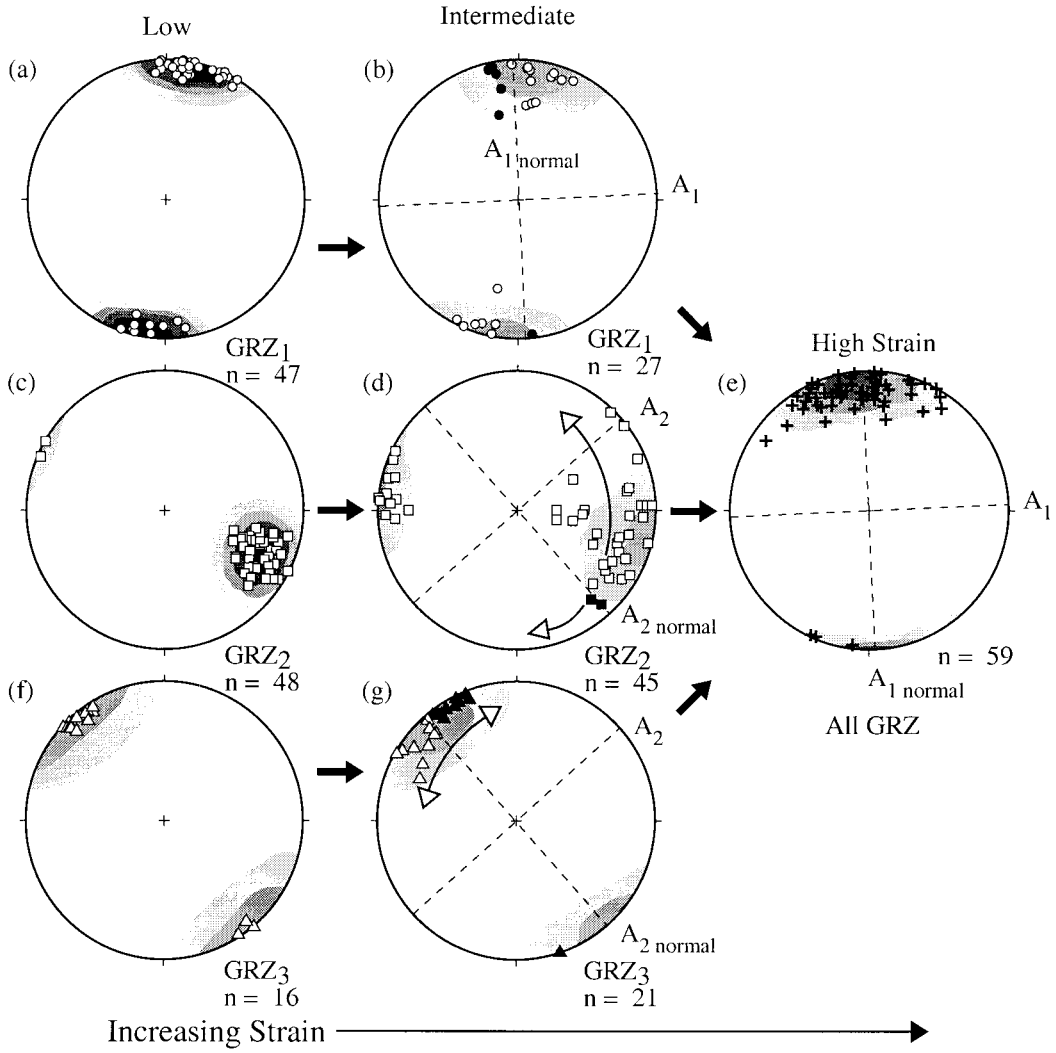

Fig. 6. Lower hemisphere equal area plots showing poles to the three sets of subvertical planar GRZs (GRZ_1, GRZ_2, GRZ_3) and their rotation history with increasing strain within the sinistral D_3 shear zones. Bold black arrows outside plots show direction of increasing D_3 strain from left to right. Contour intervals are 5% per 1% area. Circles in (a) and (b) are poles to GRZ_1 in low and intermediate strain domains, respectively. Squares in (c) and (d) are poles to GRZ_2 in low and intermediate strain domains, respectively. Triangles in (f) and (g) are poles to GRZ_3 in low and intermediate strain domains, respectively. Crosses in (e) represent poles to all reaction zones (undifferentiated) in their final orientations within high strain domains. Filled circles, squares and triangles in (b), (d) and (g), respectively represent GRZ_1, GRZ_2 and GRZ_3 reaction zones that underwent backward (dextral) rotation during bulk sinistral flow within the sinistral D_3 shear zones. Thin open arrows inside plots indicate rotation directions. Dashed lines show great circle planes of the two flow apophyses (A_1 and A_2) and their respective normal planes. See text for discussion.

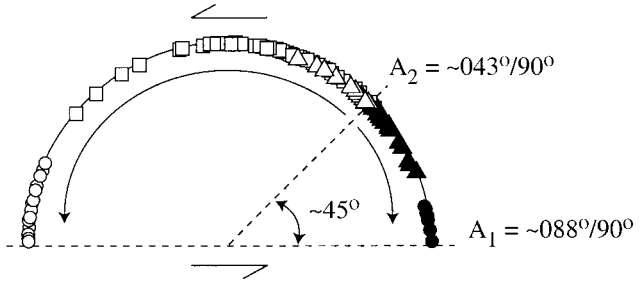

Fig. 7. Summary sketch showing variation in orientation (strikes only) and rotation sense of GRZs within D_3 flow plane (defined in text) relative to shear zone boundaries (east-striking and vertical). Circles are GRZ_1, squares are GRZ_2 and triangles are GRZ_3 reaction zones. White symbols indicate forward (sinistral) rotation, black symbols indicate backward (dextral) rotation within the sinistral D_3 shear zones.

by a mylonitic S_3 within high strain zones. Toward the edges of these small low strain pods, the oblique foliations merge into parallelism with S_3 indicating sinistral displacement (Fig. 8a). We used measures of the angle (θ) between these oblique foliations and the shear zone boundaries to estimate W_k for individual D_3 shear zones. The basis of this technique is that the orientation of the long axes of stretched grains that define the oblique foliations approaches the direction of maximum stretching for D_3 strain (Wallis, 1995; Tikoff and Fossen, 1995). Wallis (1995) provided a full description of this technique. By measuring a sufficient number (>50) of oblique foliations within a single shear zone we identified the highest angle between these foliations and the shear zone boundaries

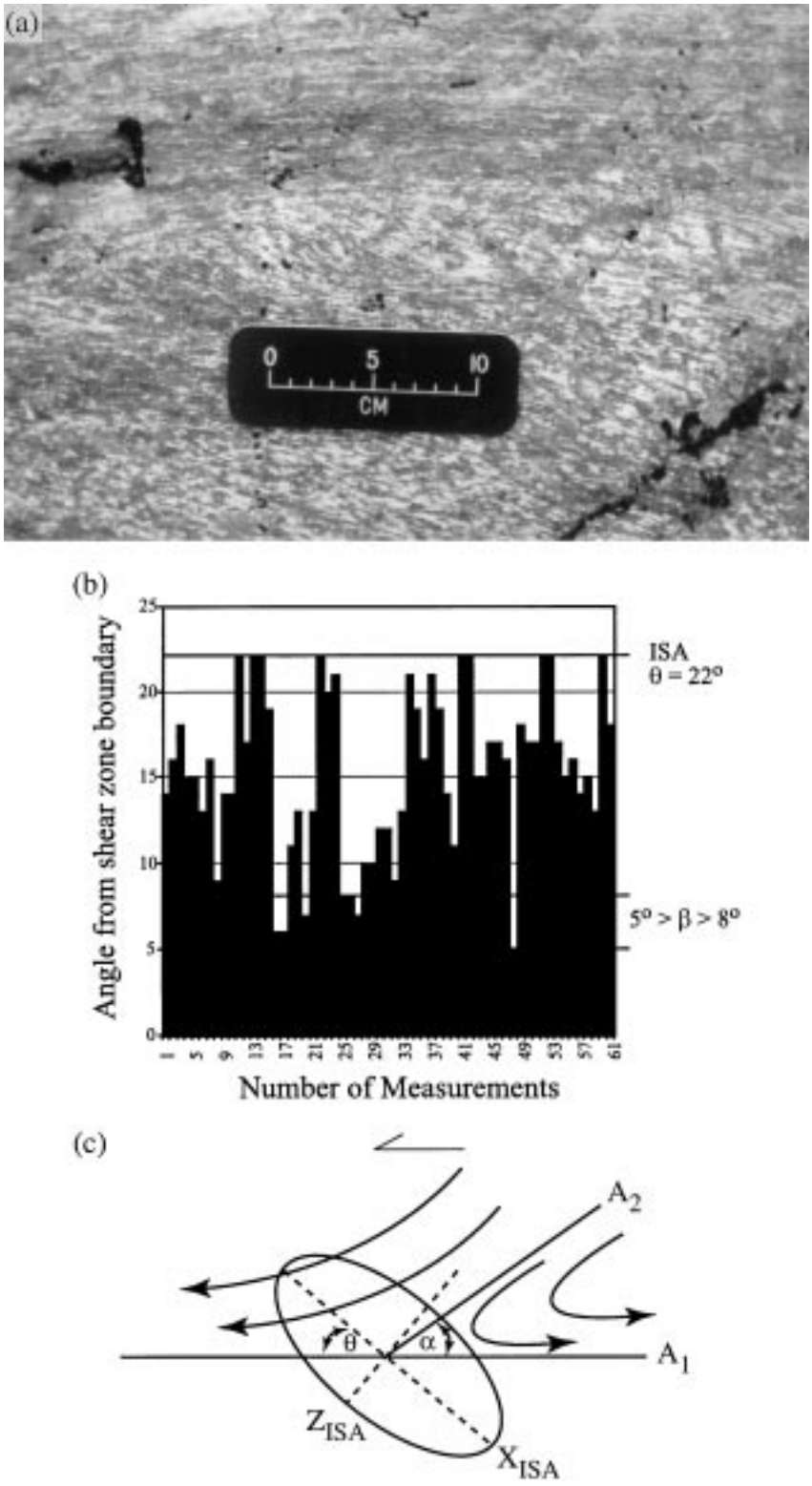

Fig. 8. (a) Sinistral D_3 shear zone showing attenuated and flattened mineral clusters that define a mylonitic foliation (S_3) at top of photo. Central part of photograph (above scale) shows an oblique foliation enveloped by mylonitic S_3 in a low strain lens. Progressive anticlockwise rotation of oblique foliation from low to high strain areas gives a sinistral shear sense for the shear zone. (b) Plot showing variation in angle between oblique foliations shown in (a) and the shear zone boundaries. See text for discussion. (c) Cartoon showing relative orientation of the flow apophyses (A_1, A_2), instantaneous strain axes (X_{ISA}, Z_{ISA}) and the angles between these elements for a sinistral pure-shear-dominated flow regime.

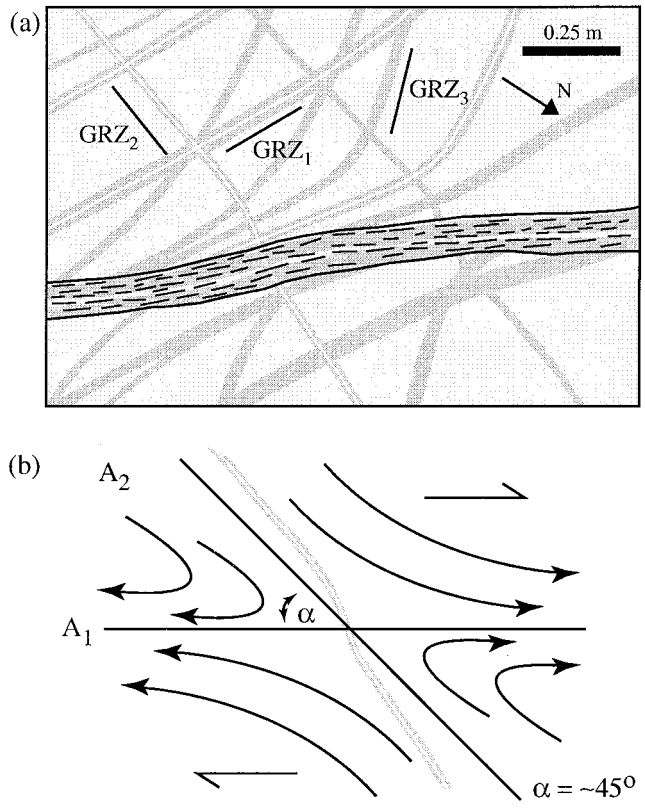

Fig. 9. (a) Plan view sketch of a dextral northwest-striking D_3 shear zone. Orientations of GRZ_1, GRZ_2 and GRZ_3 reaction zones are shown. Note that GRZ_2 reaction zones display very small amounts (<20°) of dextral rotation within the shear zone compared to other reaction zones (>60° rotation) indicating that they lie at low angles to the inclined flow apophysis (A_2). See text for discussion. (b) Interpretative cartoon showing relative orientation of flow apophyses (A_1, A_2) and the angles between these elements and the GRZ_2 lines for dextral flow regime shown in (a).

(θ_{max}) and interpreted this angle to indicate the most likely orientation of the direction of maximum instantaneous stretching. The angle θ_{max} is related to W_k as follows:

$$W_k = \sin(2\theta_{max}) \quad (2)$$

(Bobyarchick, 1986; Wallis, 1995; Tikoff and Fossen, 1995) where

$$\theta_{max} = \frac{1}{2}(90° - \nu) \quad (3)$$

where ν is the angle between the flow apophyses as defined in Section 4.1 above.

The samples we used show no evidence of annealing. Our measurements (Fig. 8b, c) suggest $\theta_{max} = 22°$ and $W_k = 0.69$.

The results obtained through an analysis of instantaneous strain agree well with our estimate of a time-average W_k using the rotated GRZs, suggesting that the estimate $W_k = 0.69$ is robust. This similarity also suggests that D_3 deformation was approximately steady-state. Furthermore, similar W_k values obtained using these different techniques provides an indirect test of the passive behavior of the GRZs. The results suggest that the reaction zones indeed behaved passively and thus provided us with a reasonable time-averaged estimate of W_k. Finally, the similarity of our two measures of W_k suggest that W_k was scale independent, such that the nature of flow for individual shear zones was similar or identical to the bulk flow regime for the entire Pembroke Valley exposures. This scale invariance is also confirmed by a third independent measure of W_k for individual shear zones. For some sinistral and dextral shear zones, we located veins that did not rotate across strain domains but passed through high strain zones weakly or virtually unaffected by the rotational component of strain (e.g., Figs. 4b, 9). In our 2D analysis, these veins are thus sub-parallel to lines of little or no rotation and provide another measure of the orientation of the inclined flow apophysis for individual dextral and sinistral shear zones. The angles of these lines (approximately 45° from shear zone boundaries) is the same as the average orientation of the flow apophyses identified by analysing all 250 veins and reaction zones, confirming our estimate of $W_k = 0.69$.

4.4. Estimates of the finite strain ratio (R_f)

Changes in the angular relationships between the three GRZ sets across strain domain boundaries and also our estimate of the orientation of the maximum stretch direction provided us with three independent means to estimate the finite strain ratio (R_f) for D_3 strain within the shear zones. In this section, we describe measurements from individual sinistral shear zones where errors could be kept at a minimum. We then compared the results from these site-specific measurements with results obtained using average angular changes displayed by all 250 measured reaction zones across the Pembroke Valley to test the validity of our results.

The first method we employed utilizes the orientation (θ_{max}) of the direction of maximum stretch with respect to the flow plane (described above), our estimate of W_k, and the orientation (β) of the maximum principal finite strain axis with respect to the flow plane. The method we used to determine β is similar to that used to find θ_{max}. We take β to coincide with the minimum angle between S_3 and the flow plane (shear zone boundary) for individual shear zones (Fig. 8b). This is a reasonable interpretation given the condition of plane strain and our analysis of the rotation of the direction of maximum stretch using oblique foliation measurements. Close inspection of all individual shear zones shows that S_3 is inclined at very low angles (5–8°) with respect to the shear zone boundaries (e.g., Fig. 8a). R_f for the shear zones can be calculated using the values of β and W_k and the solution to a standard quadratic equation discussed in detail and derived by Wallis (1995):

$$R_f = \frac{-b \pm \sqrt{b^2 - 4ac}}{2a} \quad (4)$$

where

$$a = 2W_k^2 - 2W_k^2\cos 2\beta - \sin^2 2\beta$$

$$b = -2\sin^2 2\beta$$

$$c = 2W_k^2 + 2W_k^2\cos 2\beta - \sin^2 2\beta.$$

Our measurements suggest the following values: $5° < \beta < 8°$, $W_k = 0.69$ and $\theta_{max} = 22°$. Using Eq. (4), these values yield the range: $5 < R_f < 9$ for the D_3 shear zones.

The total amount of rotation of individual GRZs during D_3 is also directly related to the R_f, assuming passive rotation. For two initially orthogonal lines (represented by the GRZ_1 and GRZ_2 sets) that have been reoriented passively by a deformation involving plane strain and no volume change, the tangent of the change in angle between these lines (tan Ψ) is a measure of the amount of shear strain (γ). The shear strain is also related to the finite strain ratio (R_f) and the final angle (ϕ') between GRZ_2 and the maximum principal axis of finite strain as follows:

$$\gamma = \frac{(R_f^2 - 1)\tan\phi'}{1 + R_f^2\tan^2\phi'} \quad (5)$$

(Ramsay and Huber, 1983; p. 294–296). The average change in angle ($\Psi = 60°$) between the initially orthogonal GRZ_1 and GRZ_2 sets for individual sinistral shear zones yielded a minimum estimate of $\gamma = 1.7$. The average angle between GRZ_1 and GRZ_2 after deformation is 30° (Fig. 4a). Together with the range $5 < \beta < 8$, these values indicate $22 < \phi' < 25$ and suggest that the minimum range of R_f is $4 < R_f < 5$ for the D_3 shear zones. This minimum estimate of R_f using Eq. (5) is in approximate agreement with the independent estimate obtained using Eq. (4).

To establish whether these estimates are also representative of the minimum average strain for the D_3 shear zones, we calculated all possible acute angles between more than 250 reaction zones from high strain domains and evaluated the results statistically (Fig. 10 and Table 2). This approach yielded a data set of more than 2000 angles and allowed us to determine average changes in the orientation of the reaction zones with increasing strain. In low and intermediate domains, the sample means and medians of all calculated angles are within 3° of each other (Table 2) indicating that the distributions of angles are not overly skewed in these domains (skewness values $\ll \pm 1$; Table 2). The acute angles in the high strain domain data set are positively skewed toward low angles (skewness = 0.89), reflecting the high degree of parallelism of garnet reaction zones in these domains as a result of the increased strain (Fig. 10c, f).

The average angle between reaction zones in each domain agrees well with those obtained by tracing individual reaction zones across strain domain boundaries. This analysis indicates that, on average, GRZ_1 and GRZ_2 form orthogonal angles in low strain domains (~93–94°) and GRZ_3 approximately bisects the angle between them (~47° from GRZ_1; Fig. 10g). Across intermediate and high strain domains, the angles between all three of these sets progressively decrease. The final orientation of GRZ_2 in high strain domains is approximately 29° with respect to shear zone boundaries (Fig. 10c, f). This measure is almost exactly identical to the measurements used in our estimation of R_f for individual shear zones. The results suggest that our estimate of R_f obtained from individual shear zones is similar to the bulk strain for the D_3 shear zones at the scale of the Pembroke Valley. The D_3 shear zones represent approximately 20–25% of the area exposed in the Pembroke Valley and our strain estimates are for this area only.

As a final check of R_f values, we obtained an estimate of R_f by using the average angular change recorded by our macroscopic analysis of GRZ_2. For this analysis, the initial (ϕ) and final (ϕ') orientation of a passively rotating line is related to R_f as follows:

$$\tan\phi' = \frac{1}{R_f}\tan\phi \quad (6)$$

(Ramsay, 1967; p. 243–244). The average initial orientation of GRZ_2 was 86° and its final orientation was 29° with respect to the shear zone boundaries. Together with our estimate of $5 < \beta < 8$, this yields $81° < \phi < 78°$; $22° < \phi' < 30°$, suggesting $12 < R_f < 13$. Taken together, our analyses suggest the approximate range $4 < R_f < 13$ for the D_3 shear zones.

Calculation of R_f using these techniques requires minimal volume or area change. We suggest that bulk volume change did not greatly affect our results. Microprobe analyses of mineral assemblages show some change in major element mineral chemistry across strain domain boundaries suggesting that some local volume or area change by the diffusion of mobile elements occurred during D_3. However, the scale (0.75 km^2) at which we measured strain greatly exceeded the length scale of diffusion within individual shear zones. Our measure of W_k using the rotation of reaction zones across the valley also is unaffected by possible volume change. No emplacement of dikes, plutons, veins or other intrusives occurred during D_3.

4.5. Estimate of the amount of lower crustal shortening during D_3

Our estimates of W_k and the range of finite strain ratios (R_f) we obtained for D_3 deformation allowed us to estimate the amount of subhorizontal shortening in shear zones affecting the lower crust during this event. The basis for this calculation is the work of Wallis (1992, 1995), who describes the relationship between W_k, R_f and the amount of stretching along the flow plane of a shear zone. This relationship can be written as follows:

$$A_1 = (T^2 - Q^2)^{1/2} + (R^2 - Q^2)^{1/2} \quad (7)$$

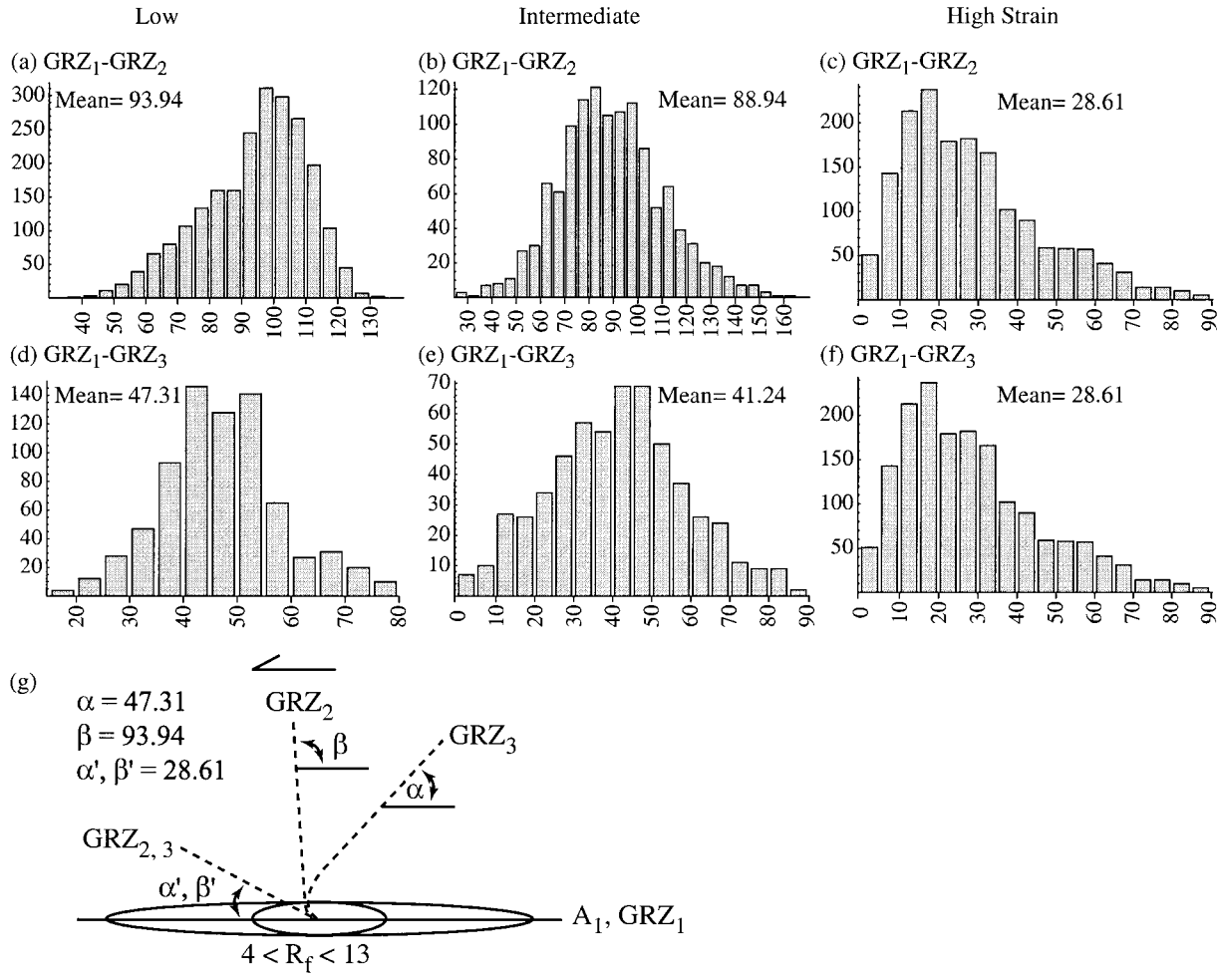

Fig. 10. (a)–(c), (d)–(f) Frequency histogram plots of all possible angles between planes for GRZ_1–GRZ_2 and GRZ_1–GRZ_3 combinations measured in the Pembroke Valley. Input data is same as that shown in Fig. 6 (measurements made about the sinistral D_3 shear zones only). (g) Schematic representation of the average orientation of GRZs and the angles they form with respect to shear zone boundaries in low strain domains (α, β) where D_3 deformation is minimal and in high strain domains (α′, β′) where D_3 deformation is at a maximum. Range of finite strain ratios (R_f) obtained in high strain domains is shown. See text for discussion.

where A_1 is the amount of stretch along the flow plane and

$$T = \frac{1}{2}(R_f^{1/2} + R_f^{-1/2}); R = \frac{1}{2}(R_f^{1/2} - R_f^{-1/2}); Q = W_k R_f$$

(Wallis, 1995, p. 1092). The amount of shortening perpendicular to the flow plane is the inverse of the stretch (Wallis, 1995). This equation can be evaluated using a Mohr circle in stretch space (see also Passchier and Urai, 1988; Wallis, 1995) where $S_1 = R_f^{1/2}$; $S_2 = R_f^{-1/2}$. Our analysis (Fig. 11) indicates that up to 60% shortening of the lower crust in high strain zones may have occurred during D_3.

Table 2
Summary of angles between planes data

Strain	Low	Intermediate	High		
Reaction zone sets	GRZ_1–GRZ_2	GRZ_1–GRZ_3	GRZ_1–GRZ_2	GRZ_1–GRZ_3	No break-down
Sample number	2256	752	1215	567	1711
Mean	93.94	47.31	88.94	41.24	28.61
Median	96.59	46.99	87.77	41.17	25.10
Standard Deviation	16.27	11.21	21.61	17.35	17.73
Sample range	90.74	60.45	142.29	87.46	88.69
Interquartile range	22.58	13.45	27.78	22.91	23.27
Skewness	− 0.57	0.27	0.24	0.12	0.89

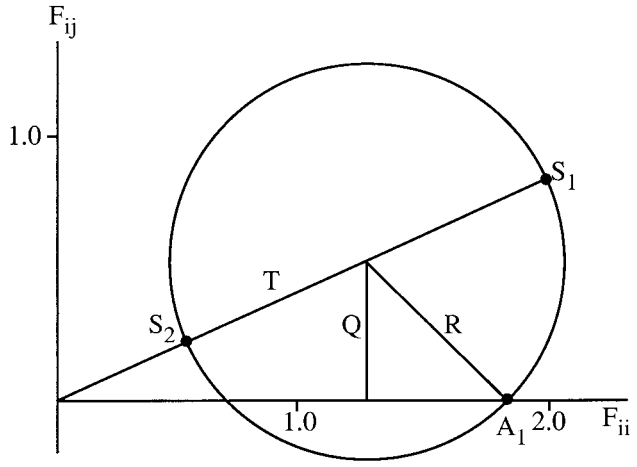

Fig. 11. Mohr diagram in stretch space representing the position gradients tensor F_{ij} (e.g. Passchier, 1988) constructed to calculate the amount of stretching and shortening within the D_3 flow plane. Parameters (S_1, S_2, Q, R, T, A_1) are defined and discussed in the text (modified from Wallis, 1995).

5. D_4: Evidence for lower crustal ductile thrust faulting

A large creek that drains the Pembroke Glacier (Fig. 5, Inset) cuts through the central part of the Pembroke Valley. This creek has carved out a ravine that provides an excellent vertical cross section of the Pembroke Granulites and vertically stacked D_4 shear zones (Fig. 12a, b). We used this exposure to examine the geometry and kinematic evolution of these shear zones in three-dimensions and to determine their effect on rocks located above and below them.

The map pattern (Fig. 5) reflects the gentle southeasterly dip of the shear zones (Fig. 12c), the topography created by the Pembroke Creek, and the narrow (~5 m) zone of mylonitic rocks that forms the central parts of the shear zones. The maximum thickness of the shallow-dipping D_4 shear zones is 6–10 m. Vertical spacing between shear zones is commonly greater than 100 m. The structurally lowest shear zone (Inset, Fig. 5) juxtaposed gabbroic orthogneisses (below) with dioritic orthogneisses that contain large (3 m wide) pods of ultramafic gneiss (above). Between individual shear zones are a heterogeneous array of curved, intersecting shear bands (Fig. 12a, b, d). Individual shear bands contain numerous kinematic indicators including C′-type shear band cleavages defined by aligned amphibole and clinozoisite, asymmetric tails on recrystallised amphibole clusters, amphibole and clinozoisite fish, oblique foliations in lower strain lenses surrounded by the main L_4–S_4 fabric, displaced GRZs, and an asymmetric deflection of the S_1 and S_3 foliations into shear band centers. Viewed on surfaces oriented perpendicular to S_4 and the shear bands, and parallel to the down-dip L_4 lineations, these structures all indicate top-up-to-the-northwest displacements. This sense of displacement and the asymmetric geometry of the shear zones and their shear bands indicate that these structures form part of a network of vertically stacked ductile thrust faults (Fig. 12a). Older fabrics in between individual thrust zones are unaffected by D_4 except for the common occurrence of minor D_4 shear bands (Fig. 5).

Inside individual 5-meter-thick thrust zones, shear bands create high strain zones that envelop lower strain lenses (Fig. 12b). Most shear bands curve and merge into parallelism with the gently dipping D_4 ductile thrust planes. Some dip to the northwest, others dip to the southeast. Despite variable dips, the sense of displacement on all shear bands surrounding the lower strain lenses is top-to-the-northwest, consistent with the bulk displacement sense of the main thrust zones. A comparison of the geometry of the foliations inside adjacent asymmetric lenses that are separated by mylonitic shear bands indicates differences in orientation (Fig. 12a, b). These differences and asymmetric kinematic indicators in the shear bands themselves suggest that these lenses moved semi-coherently relative to one another within the central parts of the main thrust zones. We have identified lenses that partially overrode adjacent lenses and form an imbricated, stacked geometry (Fig. 12b) that strongly resembles the geometry of duplexes composed of thrust horses in upper crustal thrust systems (e.g., Klepeis and Austin, 1997). A comparison of along strike variations in the geometry of these structures indicates that the effect of the relative displacement of the pods was to thicken the shear zones vertically as individual pods overrode adjacent ones during bulk top-to-the-northwest transport (e.g., Fig. 12b). Small-scale (~15 cm long) asymmetric, recumbent folds of GRZs also occur directly above thrust surfaces, reflecting high strains and vertical thickening.

6. P–T conditions of metamorphism during D_3 and D_4

In this section we estimate the conditions of metamorphism during D_3 and D_4 using mineral assemblages preserved within the gabbroic and dioritic gneisses of the Arthur River Complex. The mineral assemblages used define the S_3 and S_4 foliations. These are garnet–clinopyroxene–plagioclase–quartz–rutile–calcic amphibole–clinozoisite and garnet–biotite–plagioclase–quartz–rutile–calcic amphibole–clinozoisite, respectively. Differences in mineral chemistry in these assemblages allowed us to calculate and compare the P–T conditions using different methods. We employed experimentally calibrated geothermometers and geobarometers (Fe^{3+} corrected garnet–clinopyroxene, Ellis and Green, 1979; Krogh, 1988; garnet–hornblende, Graham and Powell, 1984; garnet–pyroxene–plagioclase–quartz, Eckert et al., 1991; garnet–hornblende–plagioclase–quartz, Kohn and Spear, 1990) and tested these results with average P–T calculations using the methods of Powell and Holland (1988, 1994). The average P–T method involves the determination of the activities of mineral end members as described by Holland (1993) and use of the computer software THERMOCALC (version 2.6; Powell and Holland, 1988; Holland and Powell, 1990; data file created April 1996). All mineral end member activities were calculated

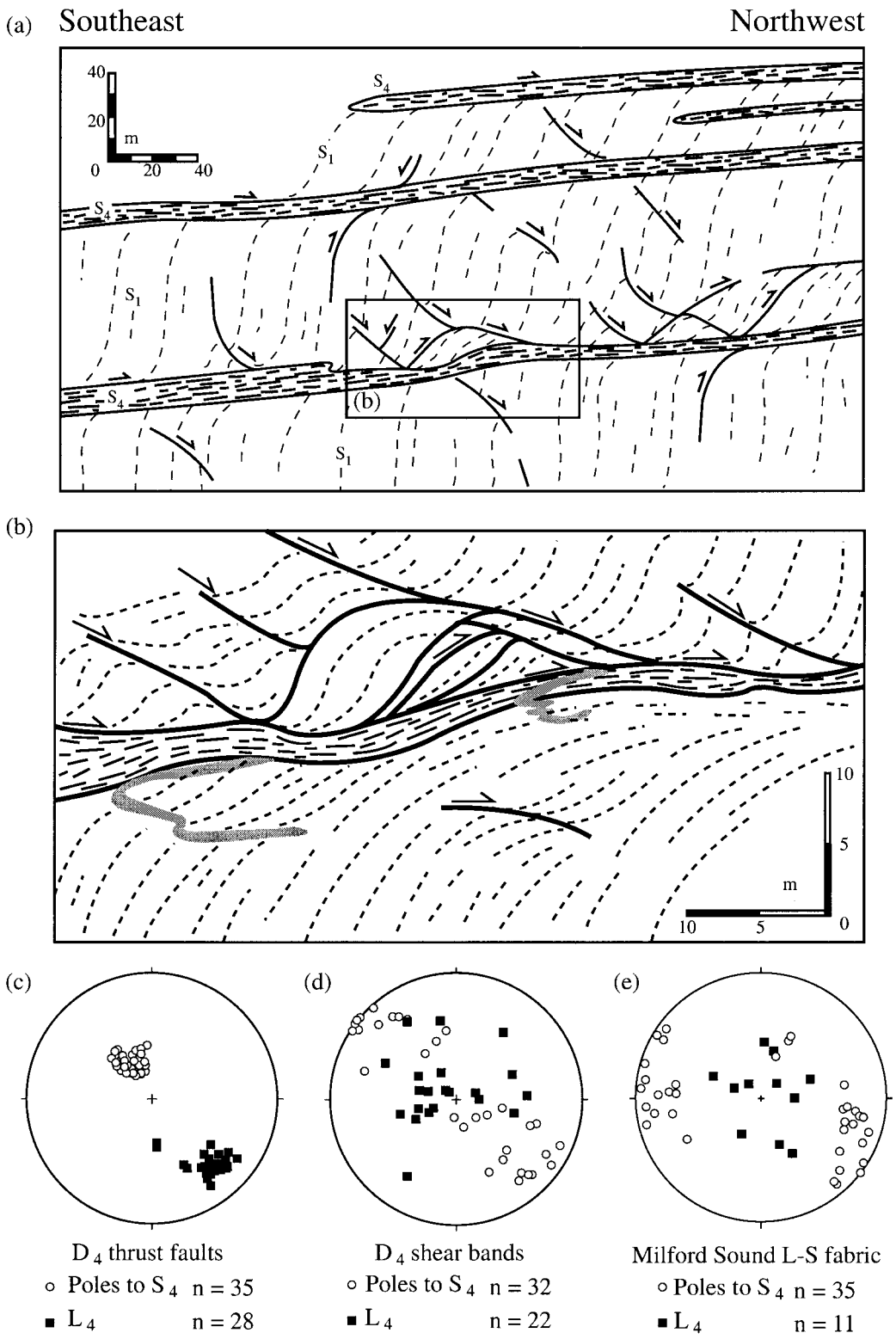

Fig. 12. (a) Vertical cross section showing the geometry of vertically stacked, gently SE-dipping D_4 shear zones and related structures. View is due west, no vertical exaggeration. Note steeply dipping D_4 shear bands that merge with main thrust surfaces. Fine dashed lines show foliation traces (S_1) between thrusts. (b) Detailed sketch of imbricate, duplex-like geometries within individual thrust zones. Bold black lines are mylonitic zones and shear bands. Shaded curved thick lines are late pegmatites. Fine dashed lines show S_1 foliation trajectories. (c) D_4 elements (L_4 and poles to S_4) from the main ductile thrust faults. (d) Elements from D_4 shear bands associated with main thrust surfaces. (e) Regional L–S tectonite fabric that forms dominant structures at Milford Sound interpreted to be related to D_4 deformation (poles to S_4 and L_4).

Table 3
Representative microprobe analyses (wt% oxide and cation data) of equilibrium assemblages

	D_3						D_4					
	Garnet	Clinopyroxene	Plagioclase	Rutile	Amphibole	Clinozoisite	Garnet	Biotite	Plagioclase	Rutile	Amphibole	Clinozoisite
SiO_2	38.91	51.95	61.71	0.03	42.71	37.35	38.36	35.94	61.92	0.02	43.60	38.78
TiO_2	0.03	0.39	0.00	98.41	0.81	0.13	0.07	0.26	0.00	97.96	0.50	0.09
Al_2O_3	21.85	6.97	23.98	0.00	12.93	25.86	21.45	18.44	23.29	0.00	13.01	27.98
Cr_2O_3	0.03	0.04	0.00	0.00	0.02	0.02	0.00	0.00	0.00	0.02	0.00	0.00
FeO	21.29	6.97	0.14	0.41	13.00	7.98	24.81	14.86	0.67	0.48	15.13	6.61
MnO	0.32	0.04	0.00	0.01	0.02	0.03	1.73	0.10	0.01	0.00	0.21	0.13
MgO	7.08	10.51	0.00	0.00	11.45	0.00	4.30	13.58	0.11	0.00	10.30	0.00
CaO	10.13	19.10	4.97	0.09	11.54	22.83	8.89	0.14	5.37	0.05	11.03	23.32
Na_2O	0.02	2.84	8.44	0.01	1.61	0.02	0.00	0.17	8.17	0.01	1.59	0.00
K_2O	0.01	0.02	0.31	0.00	0.91	0.03	0.01	8.72	0.07	0.02	0.76	0.00
Total	99.66	98.84	99.54	98.96	94.99	94.24	99.62	92.21	99.60	98.55	96.13	96.91
# oxygens	12	6	8	2	23	26	12	22	8	2	23	26
Si	2.99	1.93	2.75	0.00	6.46	6.15	3.01	5.51	2.76	0.00	6.55	6.14
Ti	0.00	0.01	0.00	1.00	0.09	0.02	0.00	0.03	0.00	1.00	0.06	0.01
Al	1.98	0.31	1.26	0.00	2.31	5.02	1.98	3.33	1.22	0.00	2.31	5.23
Cr	0.00	0.00	0.00	0.00	0.00	0.00	0.00	0.00	0.00	0.00	0.00	0.00
Fe	1.37	0.22	0.01	0.00	1.64	1.10	1.63	1.90	0.02	0.01	1.90	0.88
Mn	0.02	0.00	0.00	0.00	0.00	0.00	0.11	0.01	0.00	0.00	0.03	0.02
Mg	0.81	0.58	0.00	0.00	2.58	0.00	0.50	3.10	0.01	0.00	2.31	0.00
Ca	0.83	0.76	0.24	0.00	1.87	4.03	0.75	0.02	0.26	0.00	1.78	3.96
Na	0.00	0.20	0.73	0.00	0.47	0.00	0.00	0.05	0.71	0.00	0.46	0.00
K	0.00	0.00	0.02	0.00	0.18	0.01	0.00	1.71	0.00	0.00	0.15	0.00
Total	8.02	4.01	5.00	1.00	15.61	16.33	7.99	15.67	4.98	1.00	15.54	16.23
	$T = 676 \pm 34$°C, $P = 14.0 \pm 1.26$ kbars						$T = 674 \pm 36$°C, $P = 14.1 \pm 1.24$ kbars					

using the computer program AX (Holland, 1993) and the defaults suggested in Powell and Holland (1988). Chemical analyses were obtained using a Cameca SX50 microprobe running with an accelerating voltage of 15 kV and a beam width of 1–5 μm (representative analyses shown in Table 3).

Several observations suggest that minerals defining S_3 and S_4 formed during deformation. First, asymmetric amphibole, biotite, and clinozoisite fish indicate syntectonic mineral growth. Second, D_4 thrust zones contain garnet with curved inclusion trails consistent with syntectonic porphyroblast growth. Third, the relative timing of mineral equilibration in the D_3 and D_4 shear zones respectively, is well constrained. Biotite, for example, defines a slightly more hydrous S_4 assemblage but does not form part of the S_3 mineral assemblage, indicating syn-D_4 mineral growth. Finally, microprobe data and mineral x-ray maps also indicate that plagioclase and ferromagnesian minerals in the two shear zones display different mineral compositions (Table 3).

The results of our analyses suggest that the L_3–S_3 assemblage garnet–clinopyroxene–plagioclase–quartz–rutile–calcic amphibole–clinozoisite equilibrated at peak conditions of 14.0 ± 1.26 kbars and 676 ± 34°C and the L_4–S_4 assemblage garnet–biotite–plagioclase–quartz–rutile–calcic amphibole–clinozoisite equilibrated at peak conditions of 14.1 ± 1.24 kbars and 674 ± 36°C (Table 3). Both the directly calibrated and average P–T methods produced similar results (within error) suggesting that these estimates are robust. The results indicate that D_3 and D_4 occurred under granulite facies conditions at similar lower crustal (>45 km) levels and that high-P metamorphic conditions persisted after the formation of the granulite facies garnet reaction zones.

7. Discussion

Gabbroic and dioritic gneisses in the Pembroke Valley of northern Fiordland experienced high-P (~14 kbars) granulite facies metamorphism accompanying the formation of anorthositic veins and fracture arrays (D_2), and two phases (D_3 and D_4) of granulite facies deformation at lower crustal levels. The anorthositic veins and their surrounding garnet–clinopyroxene reaction zones are consistent with the petrologic observations of high-P metamorphism made by previous workers in Fiordland, including Blattner (1976), Oliver (1977), Oliver and Coggon (1979), Mattinson et al. (1986), Gibson et al. (1988) and Bradshaw, 1989a,b. These GRZs and veins constrain the kinematic history of D_3 and D_4 deformation following pluton emplacement and metamorphism. The results indicate that D_3 shear zones formed within a pure-shear-dominated sinistral regime ($W_k = 0.69$) leading to bulk subhorizontal shortening and NE–SW

stretching (present-day coordinates). D_4 produced a series of vertically stacked, low angle ductile thrust faults that accommodated NW-directed tectonic transport and vertical thickening of the crust. These phases of deformation occurred at identical peak conditions of 14.0 ± 1.26 kbars and 676 ± 34°C and 14.1 ± 1.24 kbars and 674 ± 36°C, respectively (Table 3).

7.1. Controls on deformation partitioning and ductile flow in the lower crust

Crystal plastic deformation processes are strongly influenced by mechanisms that contribute to strain softening during the development of shear zones (e.g., Passchier and Trouw, 1995). One important influence on the effect of strain softening is grain size, which can enhance processes such as solid state diffusion creep within deforming rocks (e.g., White et al., 1980; Passchier and Trouw, 1995). Several observations suggest that the mineralogy, orientation, and grain size of the GRZs in the Pembroke Valley influenced the geometry of ductile flow during D_3 deformation. First, the dominant sinistral set of shear zones everywhere parallels GRZ_1. Second, our 2D kinematic analysis shows that the locations of the two flow apophyses for D_3 coincide with two of the three sets of GRZs. We have established that one apophysis paralleled the boundaries of the dominant sinistral set of shear zones and the second apophysis divided the GRZ_3 set. We suggest that the orientation of the GRZ_1 set and the smaller grain size produced by granulite facies metamorphism and recrystallization in the GRZs compared to the adjacent protolith led to a preferential reactivation of the GRZ_1 set during subsequent subhorizontal shortening and sinistral sub-simple shear. In this sense, the pre-existing mineral phase and grain size heterogeneity produced by the GRZs controlled the geometry and orientation of critical flow parameters during D_3 sinistral pure-shear-dominated flow. The GRZ_1 set appears to have been preferentially oriented to accommodate subhorizontal sinistral displacements during D_3.

7.2. Oblique sinistral convergence, arc–continent collision and deformation at the roots of a convergent orogen

On the basis of geochronological and geochemical data, Muir et al. (1995, 1998) suggested that the sudden appearance of large volumes of Na-rich magma in Fiordland during the Early Cretaceous, including plutons of the Western Fiordland Orthogneiss, was triggered tectonically by the underthrusting and subsequent melting of mafic arc-related rocks (MTZ) beneath western Fiordland. This interpretation implies that major tectonic thickening and thrust faulting began prior to the emplacement of the Western Fiordland Orthogneiss and after formation of the MTZ arc. Mattinson et al. (1986), McCulloch et al. (1987), Bradshaw (1989) and Bradshaw (1989a) used metamorphic and regional geologic evidence to infer a similar scenario of tectonic thickening during arc–continent collision near the present location of the MTZ. The structural and kinematic evidence we present in this paper, representing the first discovery of large, lower crustal ductile thrust faults and sinistral, pure-shear-dominated shear zones in northern Fiordland, supports these interpretations.

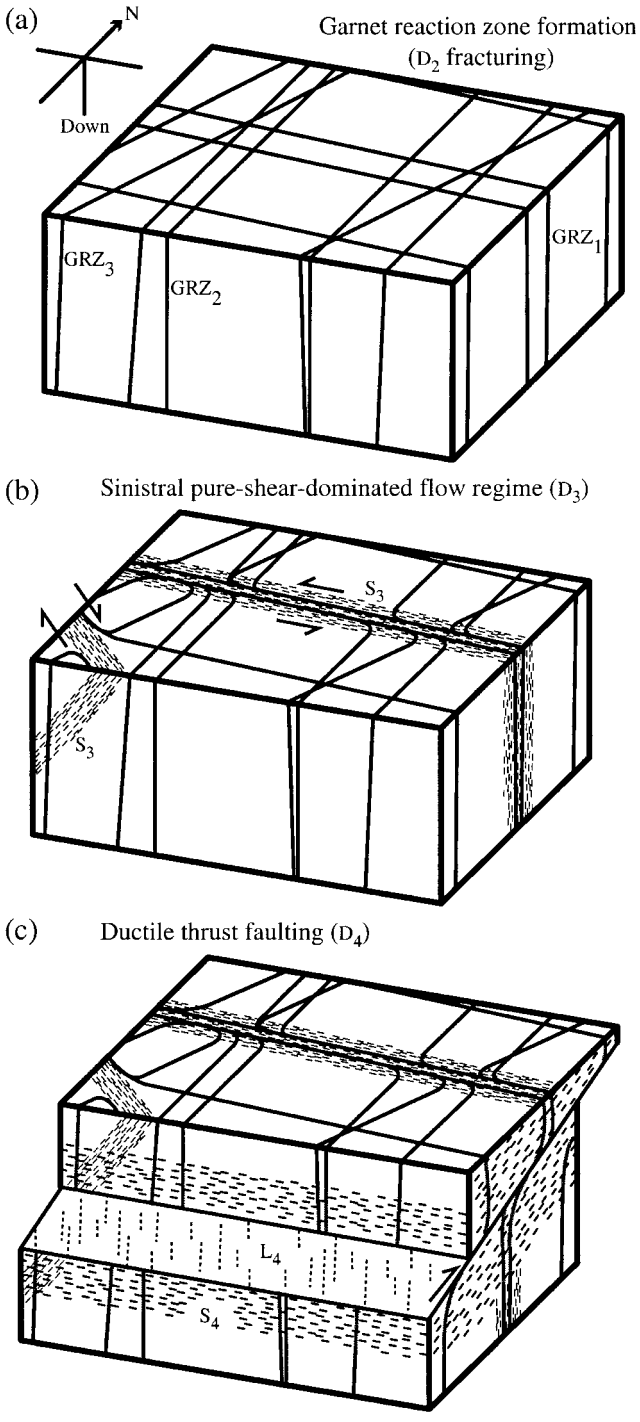

Fig. 13. Block diagrams showing (a) the relative geometry of D_2 fractures and associated GRZs, (b) sinistral pure-shear-dominated D_3 shear zones, and (c) D_4 ductile thrust faulting. Reaction zones are shown as bold black lines.

Crosscutting relationships between the structures we

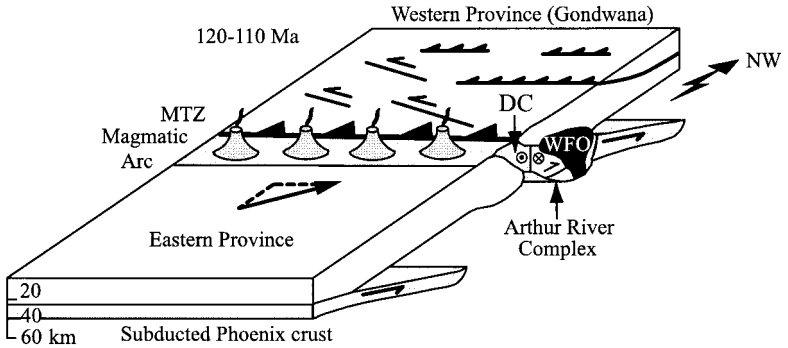

Fig. 14. Cartoon constructed for the interval 120–110 Ma showing an obliquely convergent, arc–continent collisional tectonic setting. Eastern and western provinces are shown, oblique convergence vector results in sinistral pure-shear-dominated deformation during collision of Median Tectonic Zone arc with the western province. WFO–Western Fiordland Orthogneiss; DC–Darran Complex.

describe in western Fiordland and other key features, such as other GRZs elsewhere within this belt, suggest an Early Cretaceous age for contractional deformation and high-*P* metamorphism in the Pembroke Valley. First, all high-grade fabrics exposed within the Arthur River Complex at Milford Sound are cut by a major ductile normal fault preserved inside the Anita Shear Zone (Klepeis et al., 1999). This ductile normal fault is represented by a vertically thinning shear zone that strongly contrasts in style with the older, vertically thickening D_4 thrusts we describe here. Regional correlation of extensional shear zones across Fiordland (Hill, 1995b; Klepeis et al., 1999) suggests that the dominant fabric in the Arthur River Complex and all ductile fabrics (D_1 to D_4) in the Pembroke Valley are older than 108 Ma (date from Tulloch and Kimbrough, 1989). Second, Bradshaw (1990) reported that 126–119 Ma plutons of the Western Fiordland Orthogneiss intruded the Arthur River Complex and the MTZ arc (Mortimer et al., 1999). These plutons are variably deformed by shear zones that appear similar in style to the D_3 shear zones described here (Bradshaw, 1990) although these features may not be exactly correlative in time. The same type of distinctive anorthositic veins and garnet–clinopyroxene reaction zones we observed in the Pembroke Valley also occur within the 126–119 Ma Western Fiordland Orthogneiss (Oliver, 1977; Mattinson et al., 1986; Bradshaw, 1989b). These relationships suggest that D_3 and D_4 contractional deformation occurred during the Early Cretaceous. This interpretation is also consistent with new, unpublished evidence that east-vergent ductile thrust faults deform plutons of the Western Fiordland Orthogneiss at Caswell Sound in west-central Fiordland (Daczko et al., in preparation). The implication is that major ductile thrusting and a pure-shear dominated sinistral flow regime within an obliquely convergent setting began prior to, and outlasted the emplacement of, the 126–119 Ma Western Fiordland Orthogneiss.

Our new data also suggest that a kinematic and structural link existed between deformation of the Darran Complex at upper crustal levels and deformation of the Pembroke Granulites at lower crustal levels during Early Cretaceous oblique convergence. Wandres et al. (1998) describe upper amphibolite facies sinistral shear zones recrystallizing two-pyroxene diorites within the Darran Complex that appear similar in style to the D_3 shear zones we describe here. Both the Darran Complex shear zones and the D_3 event in the Pembroke Valley have displacement directions that are slightly oblique to the NE trend of the MTZ arc. In contrast, the D_4 event we describe displays NW-trending stretching directions that are nearly orthogonal to both the NE trend of the MTZ arc and the D_3 stretching directions. These relationships and evidence that both phases involved subhorizontal shortening suggest that these two events reflect a partitioning of the arc-parallel and arc-normal components of oblique convergence onto the strike-slip component of sub-simple shear zones and ductile thrust faults, respectively (Figs. 13 and 14). This type of strain partitioning is common in obliquely convergent margins (e.g., Hervé, 1994; Tikoff and Saint Blanquat, 1997), although other factors such as simultaneous motion on linked shear zones and inherited anisotropies can influence this type of deformation partitioning at deep levels (Klepeis and Crawford, 1999). Nevertheless, our interpretation of oblique convergence (Fig. 14) is consistent with plate tectonic models involving the oblique subduction of the Phoenix plate beneath the eastern margin of New Zealand located outboard of the MTZ (e.g., Bradshaw, 1989).

Lastly, we suggest that the steeply dipping *L–S* tectonites of the western and central parts of Milford Sound are correlative with the steeply dipping foliations that occur between the stacked thrust faults in the Pembroke Valley. The strikes and trends of many of the steeply dipping foliations and down-dip mineral lineations along Milford Sound are similar to the steeply dipping and steeply plunging portions of the S_4 foliation and down-dip L_4 mineral lineations affecting the Pembroke Granulites. The conditions of metamorphism during D_4 in the Pembroke Valley also are similar to the metamorphic conditions estimated for the time of fabric development in Milford Sound (Clarke et al., 2000). We therefore suggest that contractional deformation within an

Early Cretaceous collisional setting produced the dominant fabric in the Arthur River Complex in northern Fiordland.

8. Conclusions

Dioritic and gabbroic orthogneisses in the Pembroke Valley near Milford Sound preserve evidence of high-*P* (>14 kbars) granulite facies metamorphism and two kinematically distinct phases of granulite facies deformation (D_3 and D_4). Granulite facies mineral assemblages occur in garnet–clinopyroxene-bearing reaction zones that surround a network of anorthositic veins and fracture arrays (D_2). Quantitative kinematic and metamorphic analyses of rotated vein sets, reaction zones, and shear zones indicate that D_3 was characterized by sinistral pure shear-dominated flow ($W_k = 0.69$) resulting in subhorizontal shortening and NE–SW stretching (present-day coordinates) at $P = 14.0 \pm 1.26$ kbars and $T = 676 \pm 34$°C. Estimates of strain magnitude ($4 < R_f < 13$) coupled with a time-averaged kinematic vorticity number ($W_k = 0.69$) suggest that up to 60% shortening occurred during D_3 in high strain zones of the lower crust. D_3 shear zones are overprinted by vertically stacked (~100 m spacing), gently dipping ductile thrust faults (D_4) that resulted in bulk NW-directed tectonic transport and vertical thickening at $P = 14.1 \pm 1.24$ kbars and $T = 674 \pm 36$°C. These data represent the first structural and kinematic evidence of major tectonic thickening, ductile thrust faulting and sinistral pure-shear-dominated flow at the lower crustal roots (>45 km) of a convergent orogen in Fiordland. Distinctive kinematic styles of deformation suggest that D_3 and D_4 reflect a degree of partitioning of the arc-parallel and arc-normal components of oblique sinistral convergence onto D_3 sub-simple shear zones and ductile thrust faults, respectively. Inherited structure partially controlled deformation partitioning in the lower crust during oblique convergence. We interpret these events to reflect the oblique collision of a major magmatic arc, represented by the MTZ, with the paleo–Pacific margin of Gondwana.

Acknowledgements

Funding to support this work was provided by the Australian Research Council (ARC grant A10009053 to G.L. Clarke and K.A. Klepeis, and University of Sydney Institutional Australian Research Council grants to K.A. Klepeis). An Australian Post-graduate award supported N.R. Daczko during preparation of this manuscript. We are especially grateful to Nick Mortimer and Andy Tulloch of the IGNS, Dunedin for many helpful discussions and logistical assistance, and to the Department of Conservation in Te Anau for permission to visit and sample localities in the Fiordland National Park. We also thank R.L. Turner, T. Patrick, and J. Hollis for their assistance in the field and laboratory; and Gabriela Mora and Nick Walker for many helpful discussions. We thank P. Blattner, R. Spark, J.Y. Bradshaw, J.D. Bradshaw and the numerous other New Zealand scientists whose work in northern Fiordland and elsewhere in western New Zealand set the stage for our investigation. K.A K. also thanks G.J.H. Oliver and R. Sutherland for interesting discussions on Fiordland geology. Critical reviews by B. Tikoff and G.J.H. Oliver and the careful editorial work of R.J. Norris considerably improved an earlier version of the manuscript.

References

Blattner, P., 1976. Replacement of hornblende by garnet in granulite facies assemblages near Milford Sound, New Zealand. Contributions to Mineralogy and Petrology 55, 181–190.

Blattner, P., 1978. Geology of the crystalline basement between Milford Sound and the Hollyford Valley, New Zealand. New Zealand Journal of Geology and Geophysics 21, 33–47.

Blattner, P., 1991. The North Fiordland transcurrent convergence. New Zealand Journal of Geology and Geophysics 34, 533–542.

Bobyarchick, A.R., 1986. The eigenvalues of steady flow in Mohr space. Tectonophysics 122, 35–51.

Bradshaw, J.D., 1989. Cretaceous geotectonic patterns in the New Zealand region. Tectonics 8, 803–820.

Bradshaw, J.D., 1993. A review of the Median Tectonic Zone: terrane boundaries and terrane amalgamation near the Median Tectonic Line. New Zealand Journal of Geology and Geophysics 36, 117–125.

Bradshaw, J.Y., 1989a. Origin and metamorphic history of an Early Cretaceous polybaric granulite terrain, Fiordland, southwest New Zealand. Contributions to Mineralogy and Petrology 103, 346–360.

Bradshaw, J.Y., 1989b. Early Cretaceous vein-related garnet granulite in Fiordland, southwest New Zealand: a case for infiltration of mantle-derived CO_2-rich fluids. Journal of Geology 97, 697–717.

Bradshaw, J.Y., 1990. Geology of crystalline rocks of northern Fiordland: details of the granulite facies Western Fiordland Orthogneiss and associated rock units. New Zealand Journal of Geology and Geophysics 33, 465–484.

Bradshaw, J.Y., Kimbrough, D.L., 1989. Comment: Age constraints on metamorphism and the development of a metamorphic core complex in Fiordland, southern New Zealand. Geology 17, 380–381.

Brown, E.H., 1996. High-pressure metamorphism caused by magma loading in Fiordland, New Zealand. Journal of Metamorphic Geology 14, 441–452.

Carter, R.M., Landis, C.A., Norris, R.J., Bishop, D.G., 1974. Suggestions towards a high-level nomenclature for New Zealand rocks. Journal of the Royal Society of New Zealand 4, 29–84.

Clarke, G.L., Klepeis, K.A., Daczko, N.R., 2000. Cretaceous high-*P* granulites at Milford Sound, New Zealand: metamorphic history and emplacement in a convergent margin setting. Journal of Metamorphic Geology 18, 359–374.

Eckert Jr., J.O., Newton, R.C., Kleppa, O.J., 1991. The ?H of reaction and recalibration of garnet–pyroxene–plagioclase–quartz geobarometers in the CMAS system by solution calorimetry. American Mineralogist 76, 148–160.

Ellis, D.J., Green, D.H., 1979. An experimental study of the effect of Ca upon garnet–clinopyroxene Fe–Mg exchange equilibria. Contributions to Mineralogy and Petrology 71, 13–22.

Gibson, G.M., Ireland, T.R., 1995. Granulite formation during continental extension in Fiordland. Nature 375, 479–482.

Gibson, G.M., Ireland, T.R., 1996. Extension of Delamarian (Ross) orogen into western New Zealand: Evidence from zircon ages and implications for crustal growth along the Pacific margin of Gondwana. Geology 24, 1087–1090.

Gibson, G.M., McDougall, I., Ireland, T.R., 1988. Age constraints on

metamorphism and the development of a metamorphic core complex in Fiordland, southern New Zealand. Geology 16, 405–408.

Graham, C.M., Powell, R., 1984. A garnet–hornblende geothermometer; calibration, testing, and application to the Pelona Schist, Southern California. Journal of Metamorphic Geology 2, 13–31.

Hervé, F., 1994. The southern Andes between 39° and 44°S latitude: The geological signature of a transpressive tectonic regime related to a magmatic arc. In: Reutter, K.-J., Scheuber, E., Wigger, P.J. (Eds.). Tectonics of the Southern Central Andes. Springer Verlag, New York, pp. 243–248.

Hill, E.J., 1995a. A deep crustal shear zone exposed in western Fiordland, New Zealand. Tectonics 14, 1172–1181.

Hill, E.J., 1995b. The Anita Shear Zone: a major, middle Cretaceous tectonic boundary in northwestern Fiordland. New Zealand Journal of Geology and Geophysics 38, 93–103.

Holland, T.J.B., 1993. Computer program AX. http://www.esc.cam.ac.uk/software.html

Holland, T.J.B., Powell, R., 1990. An enlarged and updated internally consistent thermodynamic data set with uncertainties and correlations; the system K_2O–Na_2O–CaO–MgO–MnO–FeO–Fe_2O_3–Al_2O_3–TiO_2–SiO_2–C–H_2O–O_2. Journal of Metamorphic Geology 8, 89–124.

Ireland, T.R., Gibson, G.M., 1998. SHRIMP monazite and zircon geochronology of high-grade metamorphism in New Zealand. Journal of Metamorphic Geology 16, 149–167.

Kimbrough, D.L., Tulloch, A.J., Coombs, D.S., Landis, C.A., Johnston, M.R., Mattinson, J.L., 1994. Uranium–lead zircon ages from the Median Tectonic Zone, New Zealand. New Zealand Journal of Geology and Geophysics 37, 393–419.

Klepeis, K.A., Austin, J.A., 1997. Contrasting styles of superposed deformation in the southernmost Andes. Tectonics 16, 755–776.

Klepeis, K.A., Daczko, N.R., Clarke, G.L., 1999. Kinematic vorticity and tectonic significance of superposed mylonites in major lower crustal shear zone, northern Fiordland, New Zealand. Journal of Structural Geology 21, 1385–1405.

Klepeis, K.A., Crawford, M.L., 1999. High temperature, arc-parallel normal faulting at the roots of an obliquely convergent orogen. Geology 27, 7–10.

Kohn, M.J., Spear, F.S., 1990. Two new geobarometers for garnet amphibolites, with applications to southeastern Vermont. American Mineralogist 75, 89–96.

Krogh, E.J., 1988. The garnet–clinopyroxene Fe–Mg geothermometer: a reinterpretation of existing experimental data. Contributions to Mineralogy and Petrology 99, 44–48.

Lamarche, G., Collot, J.-Y., Wood, R.A., Sosson, M., Sutherland, R., Delteil, J., 1997. The Oligocene–Miocene Pacific–Australia plate boundary, south of New Zealand: Evolution from oceanic spreading to strike-slip faulting. Earth and Planetary Science Letters 148, 129–139.

Lister, G.S., Williams, P.F., 1983. The partitioning of deformation in flowing rock masses. Tectonophysics 49, 37–78.

Mattinson, J.L., Kimbrough, D.L., Bradshaw, J.Y., 1986. Western Fiordland orthogneiss: Early Cretaceous arc magmatism and granulite facies metamorphism, New Zealand. Contributions to Mineralogy and Petrology 92, 383–392.

McCulloch, M.T., Bradshaw, J.Y., Taylor, S.R., 1987. Sm–Nd and Rb–Sr isotopic and geochemical systematics in Phanerozoic granulites form Fiordland, Southwest New Zealand. Contributions to Mineralogy and Petrology 97, 183–195.

Mortimer, N., 1993. Jurassic tectonic history of the Otago schists, New Zealand. Tectonics 12, 237–244.

Mortimer, N., Tulloch, A.J., Spark, R.N., Walker, N.W., Ladley, E., Allibone, A., Kimbrough, D.L., 1999. Overview of the Median Batholith, New Zealand: a new interpretation of the geology of the Median Tectonic Zone and adjacent rocks. Journal of African Earth Sciences 29, 257–268.

Muir, R.J., Weaver, S.D., Bradshaw, J.D., Eby, G.N., Evans, J.A., 1995. The Cretaceous Separation Point batholith, New Zealand: granitoid magmas formed by melting of a mafic lithosphere. Journal of the Geological Society of London 152, 689–701.

Muir, R.J., Ireland, T.R., Weaver, S.D., Bradshaw, J.D., Evans, J.A., Eby, G.N., Shelly, D., 1998. Geochronology and geochemistry of a Mesozoic magmatic arc system, Fiordland, New Zealand. Journal of the Geological Society of London 155, 1037–1053.

Norris, R.J., Koons, P.O., Cooper, A.F., 1990. The obliquely-convergent plate boundary in the South Island of New Zealand: Implications for ancient collision zones. Journal of Structural Geology 12, 715–725.

Oliver, G.J.H., Coggon, J.H., 1979. Crustal Structure of Fiordland, New Zealand. Tectonophysics 54, 253–292.

Oliver, G.J.H., 1977. Feldspathic hornblende and garnet granulites and associated anorthosite pegmatites from Doubtful Sound, Fiordland, New Zealand. Contributions to Mineralogy and Petrology 65, 111–121.

Oliver, G.J.H., 1980. Geology of the granulite and amphibolite facies gneisses of Doubtful Sound, Fiordland, New Zealand. New Zealand Journal of Geology and Geophysics 1, 27–41.

Oliver, G.J.H., 1990. An exposed cross-section of continental crust, Doubtful Sound Fiordland, New Zealand; Geophysical and Geological setting. In: Fountain, M.H., Salisbury, D.M. (Eds.). Exposed Cross-sections of the Continental Crust. Kluwer Academic, Dorgrecht, pp. 43–69.

Passchier, C.W., 1986. Flow in natural shear zones-the consequences of spinning flow regimes. Earth Planetary Science Letters 77, 70–80.

Passchier, C.W., 1987. Stable positions of rigid objects in non-coaxial flow-a study in vorticity analysis. Journal of Structural Geology 9, 679–690.

Passchier, C.W., 1988. The use of Mohr circles to describe non-coaxial progressive deformation. Tectonophysics 149, 323–338.

Passchier, C.W., 1990. Reconstruction of deformation and flow parameters from deformed vein sets. Tectonophysics 180, 185–199.

Passchier, C.W., Urai, J.L., 1988. Vorticity and strain analysis using Mohr diagrams. Journal of Structural Geology 10, 755–763.

Passchier, C.W., Trouw, R.A.J., 1995. Microtectonics. Springer Verlag, Heidelberg.

Powell, R., Holland, T.J.B., 1988. An internally consistent data set with uncertainties and correlations: 3. Applications to geobarometry, worked examples and a computer program. Journal of Metamorphic Geology 6, 173–204.

Powell, R., Holland, T.J.B., 1994. Optimal geothermometry and geobarometry. American Mineralogist 75, 367–380.

Ramsay, J.G., 1967. Folding and Fracturing of Rocks. McGraw Hill, New York.

Ramsay, J.G., Huber, M., 1983. The Techniques of Modern Structural Geology, Volume 1, Strain Analysis. Academic Press, London.

Simpson, C., De Paor, D.G., 1993. Strain and kinematic analysis in general shear zones. Journal of Structural Geology 15, 1–20.

Sutherland, R., 1995. The Australia–Pacific boundary and Cenozoic plate motions in the SW Pacific: Some constraints from Geosat data. Tectonics 14, 819–831.

Tikoff, B., Fossen, H., 1995. The limitations of three-dimensional kinematic vorticity analysis. Journal of Structural Geology 17, 1771–1784.

Tikoff, B., Saint Blanquat, M., 1997. Transpressional shearing and strike-slip partitioning in the Late Cretaceous Sierra Nevada magmatic arc, California. Tectonics 16, 442–459.

Tulloch, A.J., Kimbrough, D.L., 1989. The Paparoa metamorphic core complex, New Zealand: Cretaceous extension associated with fragmentation of the Pacific margin of Gondwana. Tectonics 8, 1217–1234.

Turner, R.L., 1998. Strain patterns and recrystallization in the lower crust; Evidence from garnet reaction zones, Fiordland, New Zealand. Unpublished B.Sc (Honours) thesis, University of Sydney.

Wallis, S.R., 1992. Vorticity analysis in metachert from the Sanbagawa Belt, SW Japan. Journal of Structural Geology 14, 271–280.

Wallis, S.R., 1995. Vorticity analysis and recognition of ductile extension in the Sanbagawa belt, SW Japan. Journal of Structural Geology 17, 1077–1093.

Wandres, A.M., Weaver, S.D., Shelley, D., Bradshaw, J.D., 1998. Change from calc–alkaline to adakitic magmatism recorded in the Early Cretaceous Darran Complex, Fiordland, New Zealand. New Zealand Journal of Geology and Geophysics 41, 1–14.

White, S.H., Burrows, S.E., Carreras, J., Shaw, N.D., Humphreys, F.J., 1980. On mylonites in ductile shear zones. Journal of Structural Geology 2, 175–187.

Wood, B.L., 1972. Metamorphosed ultramafites and associated formations near Milford Sound, New Zealand. New Zealand Journal of Geology and Geophysics 15, 88–127.